New insights into the early Bajocian (Middle Jurassic) carbon cycle perturbation

Baptiste Suchéras-Marx, Guillaume Suan, Fabienne Giraud, Emanuela Mattioli, Hassan M Khozyem, Jean-Charles Mazur, Alicia Fantasia, Jorge E Spangenberg, Thierry Adatte

New insights into the early Bajocian (Middle Jurassic) carbon cycle perturbation

Baptiste Suchéras-Marx[1], Guillaume Suan[2], Fabienne Giraud[3], Emanuela Mattioli[2], Hassan M. Khozyem[4], Jean-Charles Mazur[1], Alicia Fantasia[5], Jorge E. Spangenberg[6], Thierry Adatte[7]

[1] Aix Marseille Univ, CNRS, IRD, INRAE, CEREGE, Aix-en-Provence, France

[2] Univ Lyon, Univ Lyon 1, ENSL, CNRS, LGL-TPE, 69622 Villeurbanne, France

[3] Univ Grenoble Alpes, Univ Savoie Mont Blanc, CNRS, IRD, Univ Gustave Eiffel, ISTerre, 38000 Grenoble, France

[4] Department of Geology, Faculty of Science, Aswan University, Aswan 81528, Egypt

[5] Department of Geosciences, University of Fribourg, 1700 Fribourg, Switzerland

[6] Institute of Earth Surface Dynamics, University of Lausanne, Géopolis, CH-1015 Lausanne, Switzerland

[7] Institute of Earth Sciences, University of Lausanne, Géopolis, CH-1015 Lausanne, Switzerland

Keywords: early Bajocian, carbon isotopes, carbonate, organic matter, phosphorus, western Tethys

Abstract

Mesozoic strata record numerous negative and positive carbon isotope excursions (CIE). The Middle Jurassic records a negative ~0.5‰ CIE at the Aalenian-Bajocian boundary followed by a positive ~1.5‰ CIE covering the entire early Bajocian. Although these CIEs are recorded in northern and southern western Tethys and may reflect perturbations to the global carbon cycle, they remain to remain poorly addressed yet. In this study, we present new geochemical and sedimentological data from the Chaudon-Norante section in France and Murtinheira section in Portugal in order to better constrain the origin of the lower Bajocian CIEs. Associated with the previously published $\delta^{13}C_{bulk\ carbonate}$ we present new $\delta^{13}C_{org}$ records, as well as total

phosphorus content, phosphorus accumulation rates (AR), and $CaCO_3$, siliciclastics and organic matter data. Contrarily to previous interpretations, our results show no evidence for a carbonate production crisis during the early Bajocian. A slight increase in siliciclastics and phosphorus AR would argue for oceanic fertilization but without a parallel increase in organic matter AR. The obtained stratigraphic $\delta^{13}C_{bulk\ carbonate}$ *vs.* $\delta^{13}C_{org}$ patterns are distinctive and mimic previous box modeling results simulating an increase in productivity forced by higher rates of riverine in phosphorus and weathered-carbon input burial. The subsequent organic carbon burial produced counter-greenhouse conditions, which in turn produced a cooling by CO_2 uptake. Our results indicate that the lower Bajocian event presents several similarities with the upper Valanginian positive CIE. A tidy comparison of both events may help for a better understanding of the origin and consequence of such carbon cycle perturbations.

1. Introduction

The Jurassic and Cretaceous strata are punctuated by many positive and negative carbon isotope excursions (CIEs) that have been most often attributed to major climatic, environmental, tectonic and/or biologic perturbations (e.g., Jenkyns et al., 2002; Erba, 2004; Dera et al., 2011; Friedrich et al., 2012). Many of these CIEs mark oceanic anoxic events (OAE), relatively short-lived periods (hundreds of kyr) of widespread oxygen depletion in marine waters. Some OAEs are characterized by a negative CIE, like the Toarcian OAE (T-OAE; e.g. Hesselbo et al., 2000; Suan et al., 2010) or the early Aptian OAE (OAE 1a; e.g., Erba and Tremolada, 2004; Westermann et al., 2013). These latter OAEs were likely initiated by global warming resulting from massive ^{13}C-depleted carbon input such as methane hydrates (Hesselbo et al., 2000), thermogenic methane or volcanic CO_2 (e.g., Larson and Erba, 1999; Suan et al., 2008; Adloff et al., 2020; Matsumoto et al.,2022). In contrast, the Cenomanian-Turonian OAE (OAE 2) is characterized by a marked positive CIE, the widespread occurrence of organic-rich deposits, and oxygen-depleted sedimentary facies (e.g., Schlanger et al., 1987; Bomou et al., 2013). This latter event also likely occurred during a global warming trend (e.g., Friedrich et al., 2012) interrupted by a temporary cooling, possibly driven by increased organic

carbon burial (Jarvis et al., 2011). This positive CIE has been classically linked to increased primary productivity and organic carbon burial, removing ^{13}C-depleted organic matter from the oceanic reservoir. OAE2 was hence likely initiated by an increase in export productivity that has been linked to a rapid increase in weathering and hence in nutrient input to oceanic waters (Blätter et al., 2011; Monteiro et al., 2012; Pogge von Strandmann et al., 2013) or by increased fertilization from large upwelling areas (Trabucho Alexandre et al., 2010).

Although the geochemical expression of these Mesozoic events is different and are evidently either associated with positive or negative, they have not been evenly studied yet. The CIE related to the T-OAE, the Weissert event (late Valanginian) and the OAE 2 have been recorded in many inorganic and organic substrates from various depositional settings, where independent biotic and geochemical proxies have also been generated. In comparison, the lower Bajocian records two CIE that are under-documented although those might correspond to global lithospheric, climatic and biogeochemical perturbation. The former event is a ~0.5‰ $\delta^{13}C$ negative CIE documented in several localities close to the Aalenian-Bajocian boundary, as initially shown by Bartolini et al. (1999) who recorded such an excursion in bulk carbonate from central Italy. More recently, such an event has been also recorded in bulk carbonate from Spain (O'Dogherty et al., 2006), Portugal (Suchéras-Marx et al., 2012), Saudi Arabia and Oman (Al-Mojel et al., 2018), but it is absent in available bulk carbonate records in France and Morocco (Suchéras-Marx et al., 2013; Bodin et al., 2017). A negative CIE has also been reported in belemnite calcite in Murtinheira section (Lusitanian Basin, Portugal) and in the Trotternish section (Isle of Skye, Scotland) (Jenkyns et al., 2002), but both records are difficult to discuss due to a poor biostratigraphical precision in the samples from Portugal (see fig. 7 in Jenkyns et al., 2002) and to the record of a single negative value in the upper part of the section – at the end of the Discites ammonite Zone, first ammonite Zone of the Bajocian – in Scotland. Importantly, a >2‰, negative CIE is documented in fossil wood (coal and charcoal) from the poorly dated mixed marine and fluvio-deltaic strata putatively attributed to the Aalenian-Bajocian boundary in Yorkshire, UK (Hesselbo et al., 2003), suggesting that the corresponding

carbon cycle perturbation has impacted both the oceanic and the atmospheric carbon reservoirs.

The large positive CIE first documented by Corbin (1994) and Bartolini et al. (1996) in the lower Bajocian is better documented. This CIE covers the entire lower Bajocian with the positive shift interval corresponding to the Discites (i.e., earliest lower Bajocian ammonite Zone) to top of Propinquans (i.e., third lower Bajocian ammonite Zone, also called Sauzei) ammonite zones, and the plateau interval covers the whole Humphriesianum (i.e., fourth and latest lower Bajocian ammonite Zone) ammonite Zone. The return to pre-excursion $\delta^{13}C$ values is recorded in upper Bajocian strata, within the Niortense ammonite Zone (i.e., earliest upper Bajocian ammonite Zone). This $\delta^{13}C$ positive excursion is essentially recorded in western Tethys sites, namely in France (Corbin, 1994; Brigaud et al., 2009), Italy (Bartolini et al., 1996; Bartolini et al., 1999), Portugal (Suchéras-Marx et al., 2012), Spain (O'Dogherty et al., 2006; Aguado et al., 2017) and Morocco (Bodin et al., 2017). The $\delta^{13}C$ positive excursion was recently documented in the Arabian platform of the southwestern Tethys (Al-Mojel et al., 2018). This positive CIE was reported in several bulk carbonate records (all above references), in belemnite calcite from the Isle of Skye in Scotland (Jenkyns et al., 2002) and, more recently, in brachiopod calcite from the Murtinheira section in Portugal (Ferreira et al., 2019). However, the lower Bajocian CIE has been also recorded in organic carbon material in several localities in Morocco (Bodin et al., 2017; Bodin et al., 2020), therefore bringing some insights into the geographical extent of the carbon cycle perturbation in organic material. The magnitude of the perturbation in bulk carbonate ranges from ~0.5‰ in Portugal up to ~3‰ in Saudi Arabia but is comprised between 1‰ and 1.5‰ in most localities. It ranges about 3‰ in organic matter in Morocco, the sole region with such data. The positive CIE is timely concomitant with possible global temperature decrease based on glendonite records in high latitudes (Price, 1999) or global temperature increase according to belemnites $\delta^{18}O$ (Dera et al., 2011). This time interval also records important lithospheric changes with the Pacific plate formation (Bartolini and Larson, 2001), the Alpine Tethys opening (Bill et al., 2001), and an accelerated spreading rate in the Central Atlantic (Labails et al., 2010). Finally, this time interval also witnesses an

important turnover in ammonite biodiversity (O'Dogherty et al., 2006), a relevant diversification of coccolithophores (Cobianchi et al., 1992; Suchéras-Marx et al., 2015; Giraud et al., 2016) and of dinoflagellate (Wiggan et al., 2017) groups.

The current documentation of the lower Bajocian CIEs is insufficient to develop a satisfactory mechanistic model of the underlying carbon cycle perturbations. In this study, we attempt to document more thoroughly the lower Bajocian carbon isotope composition and sedimentation rates. The results presented here are based on the Chaudon-Norante section (Subalpine Basin, France) and the Murtinheira section at Cabo Mondego (Lusitanian Basin, Portugal) deposits (Fig. 1) with both bulk carbonate and organic matter carbon isotopes, phosphorus, calcium carbonate, organic matter, and siliciclastic accumulation rates following latest age models. These data are combined with published primary productivity records to discuss the impact of sedimentation rates and phosphorus input on the carbon isotopic composition of both oceanic biosphere and oceanic reservoirs.

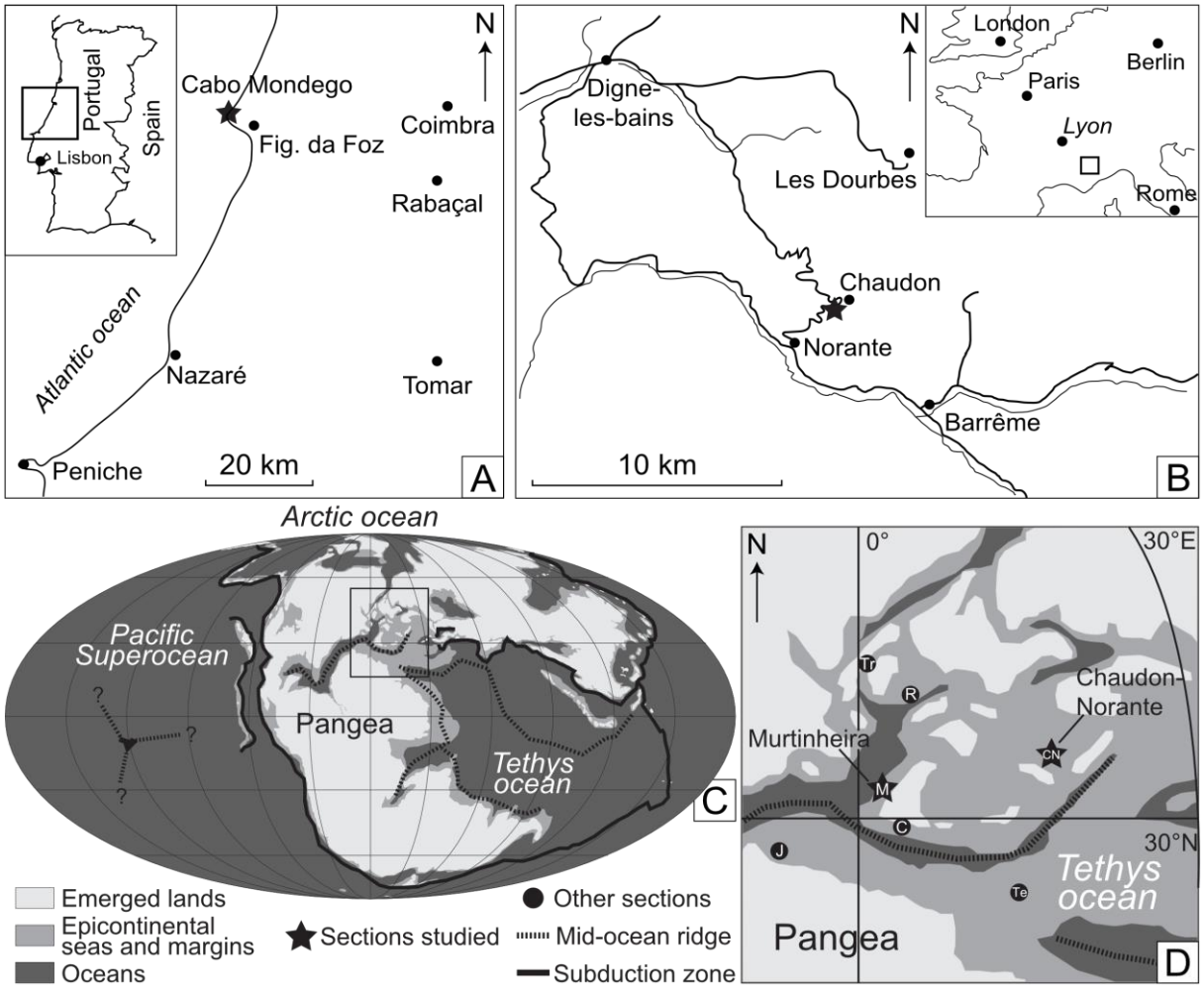

Fig. 1: Location (star) of (A) the Murtinheira section at Cabo Mondego, Portugal and (B) the Chaudon-Norante section, France. C. World paleogeographic map derived from Blakey (2008). D. Western Tethys paleogeographic map derived from Blakey (2008) showing the location of Murtinheira and Chaudon-Norante and of other sections discussed in the text: Tr. Trotternish, Scotland; R. Ravenscar Group composite section, England; C. Casa Blanca, Spain; Te. Terminilletto, Italy; J. Jebel Bou Kendill, Morocco.

2. Geological settings

2.1. Murtinheira section at Cabo Mondego

The Murtinheira section at Cabo Mondego is located on the Atlantic coast of Portugal near Figueira da Foz in the Lusitanian Basin (Fig. 1A). The Lusitanian Basin was open toward the north, the south and the west and bounded eastward by the Iberian Meseta and the Lusitanian

carbonate platform (Fig. 1C-D). This section exposes a key Middle Jurassic succession chosen as the global stratotype section and point (GSSP) of the Bajocian (Pavia and Enay, 1997) and the auxiliary stratotype section and point (ASSP) of the Bathonian (Fernandez-Lopez et al., 2009). The section age model is based on ammonite (Ruget-Perrot, 1961; Fernandez-Lopez et al., 1988; Henriques et al., 1994) and nannofossil (Ferreira et al., 2019) biostratigraphy. The studied interval is spanning the uppermost part of the upper Aalenian (Concavum ammonite Zone) to the upper part of the lower Bajocian (Humphriesianum ammonite Zone) and is composed of alternations of limestones and marlstones (Fig. 2). A more exhaustive description of the section is presented in Suchéras-Marx et al. (2012) alongside with the $CaCO_3$ (wt%) and the $\delta^{13}C_{bulk\ carbonate}$ data.

2.2. Chaudon-Norante section

The Chaudon-Norante section is located in southeastern France in the Ravin de Coueste near Digne-les-Bains in the Subalpine Basin (Fig. 1B). The French Subalpine Basin was bounded northward by the Jura carbonate platform, westward by the Central Massif and the Ardèche carbonate platform, and southward by the Provence carbonate platform (Fig. 1C-D). Unfortunate candidate for the GSSP of the Bajocian, the Chaudon-Norante section age model is based on ammonite (Pavia, 1983) and nannofossil (Erba, 1990) biostratigraphy. The studied interval is spanning the uppermost part of the Aalenian (Concavum ammonite Zone) to the upper part of the lower Bajocian (Humphriesianum ammonite Zone) and is composed of alternations of limestones and marlstones / calcareous to argillaceous marlstones (Fig. 3). A more exhaustive description of the section is presented in Suchéras-Marx et al. (2013) alongside with the $CaCO_3$ (wt%) and the $\delta^{13}C_{bulk\ carbonate}$ data.

3. Analytical methods and calculation

3.1. Organic matter analysis: TOC and $\delta^{13}C_{org}$

A total of 80 samples (32 samples from Murtinheira and 48 samples from Chaudon-Norante) were analyzed for their total organic carbon (TOC) contents and carbon isotope composition

of organic matter ($\delta^{13}C_{org}$). The analyzed samples correspond to limestones, argillaceous limestones, calcareous marlstones, marlstones or argillaceous marlstones. Prior to analysis, around 500 mg of powdered bulk sediment was mixed in 2 mL of distilled water and 5 to 8 mL of 2N HCl and react overnight at ambient temperature to remove calcium carbonate. The residue was rinsed with distilled water and centrifuged twice to remove the supernatant, reacted again with 2 mL of distilled water and 5 to 8 mL of 2N HCl and left overnight in a 90-95°C water bath to remove more refractory inorganic carbon phases. The residue was finally rinsed three times with distilled water to reach neutrality and oven-dried at 50°C.

The TOC was measured by gas chromatography using an elementary analyzer Thermo-Finnigan Flash EA 1112 at the Université de Lausanne, Switzerland. The TOC is expressed in weight percent of the rock analyzed (wt.%) and the uncertainty is about 0.1 wt.%. The carbon isotopic ratio $\delta^{13}C_{org}$ was measured using a Thermo Fischer Scientific Delta V Plus isotope ratio mass spectrometer at the Université de Lausanne, Switzerland. The results were standardized using Glycine, Urea, Graphite-24 and Pyridine and are expressed in per mil Vienna Pee Dee Belemnites (‰ VPDB).

3.2. Total phosphorus content

A total of 193 samples (79 samples from Murtinheira and 114 from Chaudon-Norante) were analyzed for their total phosphorus contents (P_{tot}) using the ascorbic acid method (Mort et al., 2007). About 100 mg of powdered bulk sediment for each sample was first dried at 45°C. Once dry, 1 mL of $MgNO_3$ was mixed to the samples and heat in a furnace at 550°C for 2 h. Once cooled, the residue was reacted with 10 mL of 1N HCl for 16 h under constant shaking. The solution was filtered with a 63 μm filter and diluted 10 times. The filtered solution was then mixed with ammonium molybdate and potassium antimonyl tartrate forming phosphomolybdic acid. This acid was reduced with ascorbic acid forming a deep blue liquid. The total phosphorus content depends on the intensity of the blue color, which was measured using a Perkin Elmer UV/Vis Spectrophotometer Lambda 25. The concentration of PO_4 was determined by

194 calibration with standard solutions (BD47 and NU81) with known concentration, is expressed
195 in mg/g.
196

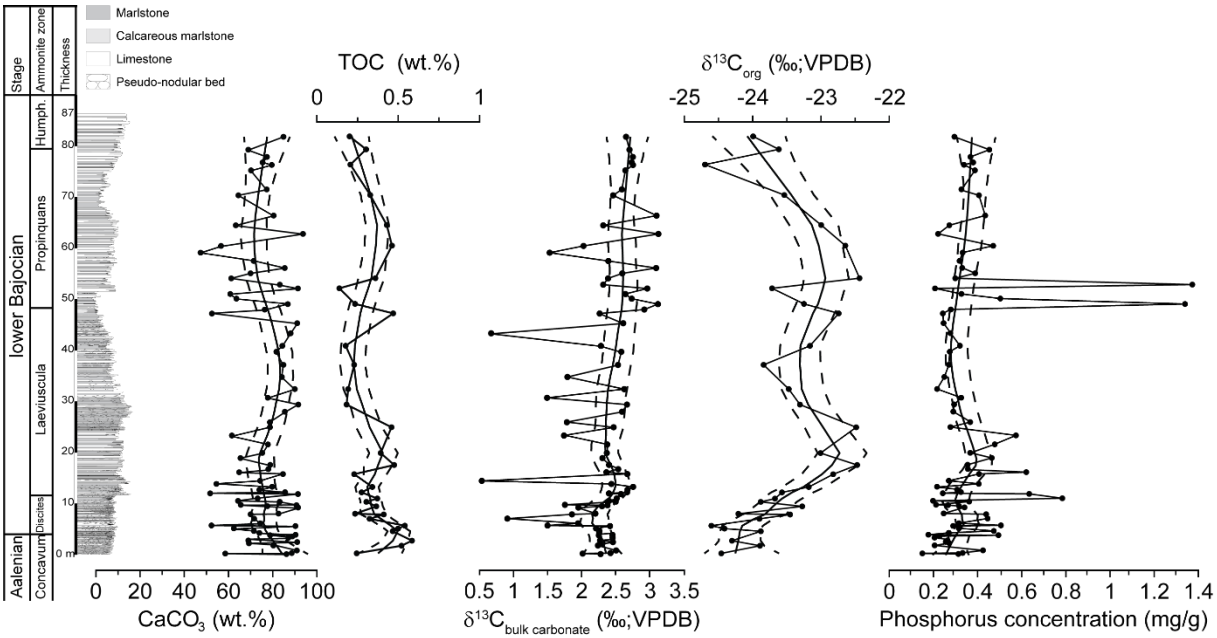

197

198 Fig. 2: Stratigraphic variations of $CaCO_3$ (wt.%), TOC (wt.%), $\delta^{13}C_{bulk\ carbonate}$ (‰, VPDB),
199 $\delta^{13}C_{org}$ (‰, VPDB) and phosphorus concentration (mg/g) in the Murtinheira section.
200 The thin lines show the LOESS-smoothed curves (smoothing factor of 0.3) and the 95%CI
201 (dashed lines) calculated using PAST3 (Hammer et al., 2001).
202

203 3.3. Accumulation rates

204 Using both available $CaCO_3$ data for both sections (from Suchéras-Marx et al., 2012; 2013)
205 and TOC and [P] quantified in this study, a set of derived accumulations rates (AR; $g/m^2/a$)
206 were calculated. Sedimentation rates (SR; m/Ma) were determined using the
207 astrochronological time scale previously obtained at Chaudon-Norante by Suchéras-Marx et
208 al. (2013; alternative solution based on Gradstein et al. 2020 in supplementary data). SR was
209 computed at the scale of ammonite Zones in order to apply the same calculation in both
210 Chaudon-Norante and Murtinheira. The calculated variables are the $CaCO_3$ AR,
211 Siliciclastics AR, C_{org} AR and PAR (i.e., Phosphorus AR). C_{org} AR was calculated based on
212 TOC, whereas Siliciclastics AR is calculated as the residues of the sum of $CaCO_3$ AR and

213 C_{org} AR. The dry bulk rock density was calculated based on the $CaCO_3$ (wt.%)/Density linear
214 relation established in both sections by Suchéras-Marx et al. (2014):
215 $[CaCO_3] \times SR \times Density = CaCO_3$ AR
216 $[TOC] \times SR \times Density = C_{org}$ AR
217 $[P] \times SR \times Density = PAR$
218 $(1 - [CaCO_3] - [TOC]) \times SR \times Density =$ Siliciclastics AR
219
220 4. Results
221 4.1. Relative concentrations and isotopic records
222 4.1.1. The Murtinheira section (Fig. 2)
223 The TOC values at Murtinheira are very low, ranging from 0.14 to 0.58 wt.%, and show a
224 general decreasing trend stratigraphically upwards, with the highest values recorded near the
225 Aalenian-Bajocian boundary. The lower part of the Laeviuscula ammonite Zone records few
226 higher values around 0.5 wt.%, whereas minimum values are recorded in the middle and upper
227 part of the Laeviuscula ammonite Zone. Overall, TOC and $CaCO_3$ contents (Figs. 2 and 3) are
228 negatively correlated, and TOC is very low, indicating that TOC values are mostly controlled
229 by a variable dilution by calcium carbonate contents.
230 Organic carbon isotope values ($\delta^{13}C_{org}$) values range between −22.4‰ and −24.7‰, with the
231 lowest values occurring in the Concavum and lower part of the Discites ammonite zones, and
232 maximum value occurring in the Propinquans ammonite Zone. The $\delta^{13}C_{org}$ values increase
233 markedly by about ~2 ‰ across the transition between the Discites–Laeviuscula ammonite
234 zones and decrease down to −24.7‰ at the end of the Propinquans ammonite Zone. The
235 overall pattern can be described as a ~2‰ positive CIE from the Aalenian to the Propinquans
236 ammonite Zone, interrupted by a ~1‰ negative CIE in the upper part of Laeviuscula ammonite
237 Zone, and followed by a second ~1‰ negative CIE in the upper part of the Propinquans
238 ammonite Zone. Based on organic matter observations of 8 samples in light microscopy, the
239 palynomorphs at Murtinheira are dominated by opaque phytoclasts, with subordinate amounts

of translucent phytoclasts and rare terrestrial sporomorph (spore and pollen grains) and rare marine palynomorphs (dinoflagellate cysts).

Phosphorus contents [P] record markedly different stratigraphic patterns. Most values are comprised between 0.2 and 0.5 mg/g, except few samples recording higher concentration (up to 1.37 mg/g). The [P] show a poor linear correlation with $CaCO_3$ or TOC contents (r = −0.03). The smoothed [P] profile shows two intervals of increasing values within the Discites ammonite Zone and in the lower part of the Laeviuscula ammonite Zone. Phosphorus contents decrease down to around 0.3 mg/g in the middle part of the Laeviuscula ammonite Zone and increase gradually up to almost 0.4 mg/g in the lowermost part of the Humphriesianum ammonite Zone. The [P] show a poor linear correlation with $CaCO_3$ or TOC contents (r = −0.03; Fig. 3).

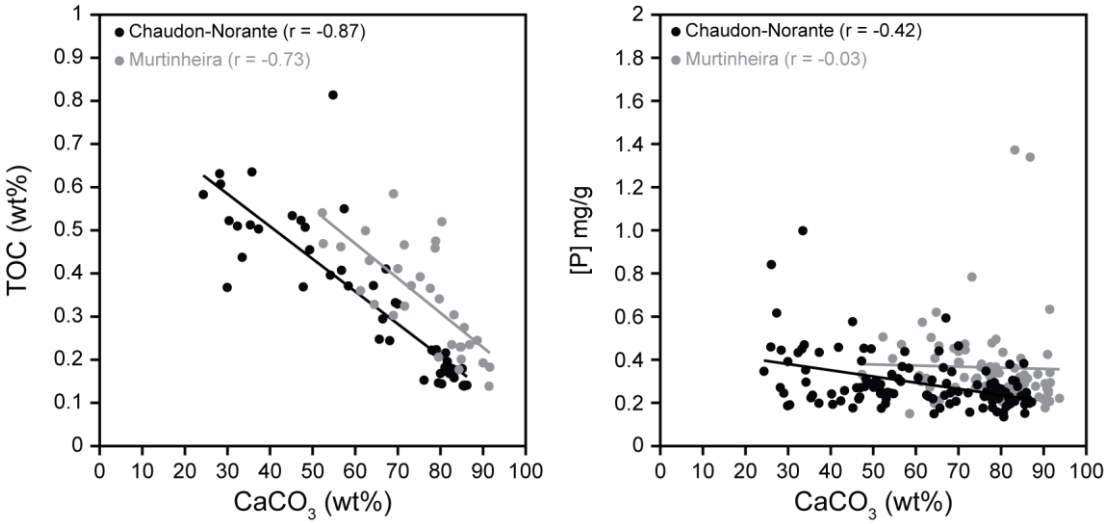

Fig. 3: $CaCO_3$ (wt.%) *versus* TOC (wt.%) plot (left-hand side) and $CaCO_3$ (wt.%) *versus* [P] (mg/g) plot (right-hand side) with Chaudon-Norante samples in black and Murtinheira samples in grey. There is a clear negative linear correlation between $CaCO_3$ and TOC values, with marlstones being more enriched in organic carbon. However, TOC is low suggesting important effect of measurement uncertainties which is about 0.1 wt.%. There is no relationship between $CaCO_3$ and [P] values at Murtinheira, whereas a moderately good negative linear correlation is apparent for Chaudon-Norante, with marlstones being slightly enriched in [P].

4.1.2. The Chaudon-Norante section (Fig. 4)

At Chaudon-Norante, TOC contents are comparable to Murtinheira with values ranging from 0.14 wt.% to 0.81 wt%. The TOC contents have higher concentrations in marlstones than in limestones (Figs. 3 and 4). The phosphorus concentration is ranging between 0.1 and 0.5 mg/g, with the exception of few samples reaching almost 1 mg/g. Both the raw and smoothed [P] profiles show a slight increase around the Discites-Laeviuscula ammonites zones boundary (Fig. 4). The [P] shows a moderately good negative linear correlation with $CaCO_3$ contents ($r = -0.42$) but there are no clear stratigraphic trends.

The $\delta^{13}C_{org}$ values range between −24.5‰ and −27‰, with lowest values occurring in the Concavum ammonite Zone and highest values occurring in the upper part of the Laeviuscula ammonite Zone (Fig. 3). The $\delta^{13}C_{org}$ profile shows a first increasing trend within the Concavum ammonite Zone interrupted by a negative CIE around the Aalenian-Bajocian boundary, values increase again by 2‰ in the Discites and Laeviuscula ammonite zones up to a maximum around the Laeviuscula-Propinquans ammonite zones boundary. The $\delta^{13}C_{org}$ values then decrease up to the top of the section, thus forming a broad, 2‰ positive CIE, but do not reach pre-excursion values (Concavum ammonite Zone and at the Aalenian-Bajocian boundary). Based on organic matter observations of 8 samples in light microscopy, the palynomorphs at Chaudon-Norante are dominated by phytoclasts (opaque and translucent) and amorphous organic matter, with rarer terrestrial sporomorphs (spore and pollen grains) and marine palynomorphs.

4.2. Accumulation rates

4.2.1. The Murtinheira section (Fig. 5)

The SR determined at the ammonite Zone level show lowest values of ~ 11.5 m/Myr in the Discites Zone. This interval is also marked by low wt.% $CaCO_3$, resulting in an important drop in $CaCO_3$ AR. The low phosphorus AR results from the drop in sedimentation rate despite the increase in phosphorus concentration. The Laeviuscula Zone conversely has the highest sedimentation rates. Hence, all sedimentary fractions considered here are increasing in terms

of accumulation rates. However, only $CaCO_3$ AR is very high all along this ammonite Zone. The siliciclastics AR, C_{org} Ar and phosphorus AR show a peak in the lower part of the Laeviuscula ammonite Zone. Finally, in the Propinquans ammonite Zone, two disctinct patterns are observed. The $CaCO_3$ and phosphorus ARs tend to increase between the base and the top of the ammonite Zone. Conversely, siliciclastics and C_{org} ARs tend to decrease between the base and the top of this ammonite Zone. Overall, siliciclastics and C_{org} ARs have very similar trends and $CaCO_3$ is the most important sediment component in term of accumulation rates. Finally, C_{org}/P_{tot} (molar ratio) is always below the Redfield ratio 1:106. Alternative results using Gradstein et al. (2020) age model is presented in supplementary material (Supplementary fig. 1). This solution is not described in this study.

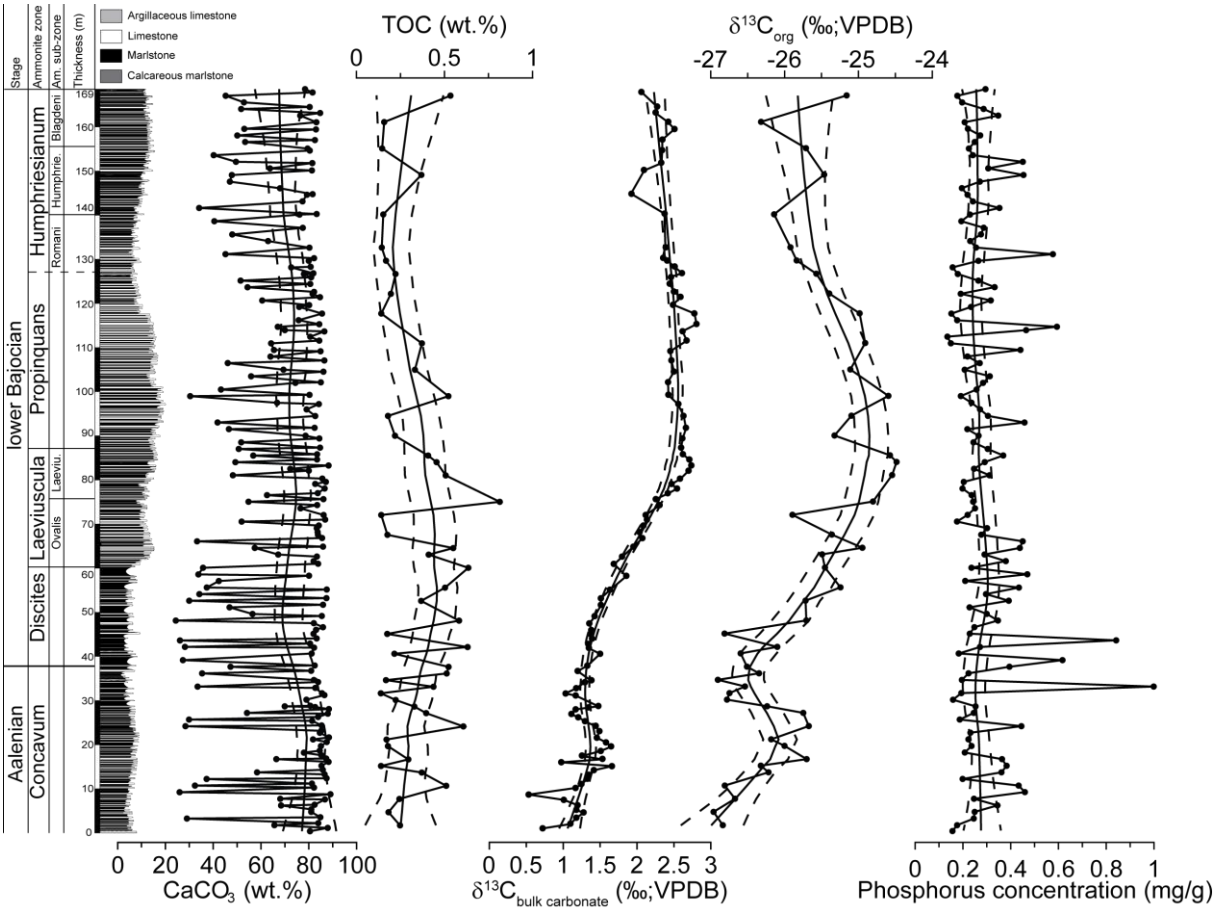

Fig. 4: Stratigraphical variations of $CaCO_3$ (wt.%), TOC (wt.%), $\delta^{13}C_{bulk\ carbonate}$ (‰, VPDB), $\delta^{13}C_{org}$ (‰, VPDB) and phosphorus concentration (mg/g) at Chaudon-Norante.

The thin lines show the LOESS-smoothed curves (smoothing factor of 0.3) and the 95%CI (dashed lines) calculated using PAST3 (Hammer et al., 2001).

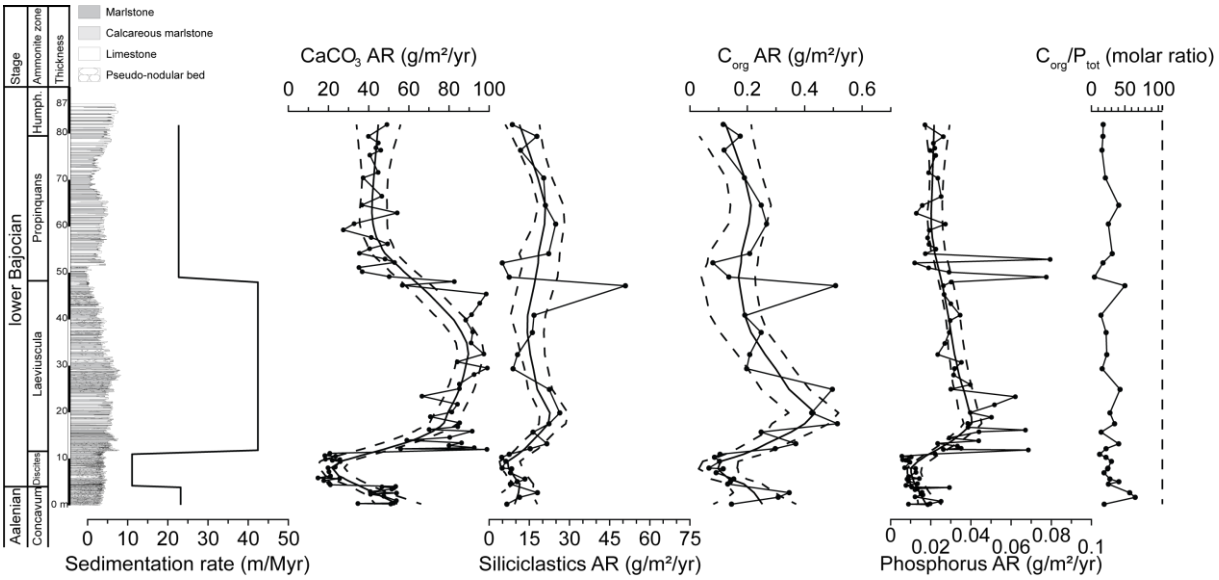

Fig. 5: Stratigraphic changes in sedimentation rate at Murtinheira (based on Suchéras-Marx et al., 2013 age model) and the resulting $CaCO_3$ accumulation rates (AR; g/m²/a), Siliciclastics AR (g/m²/a), C_{org} AR (g/m²/a), and phosphorus AR (g/m²/a), along the C_{org}/P_{tot} molar ratio. The thin lines show the LOESS-smoothed curves (smoothing factor of 0.3) and the 95%CI (dashed lines) calculated using PAST3 (Hammer et al., 2001). The dashed line in C_{org}/P_{tot} data corresponds to the Redfield ratio (1:106).

4.2.2. The Chaudon-Norante section (Fig. 6)

The age model for the lower Bajocian from Suchéras-Marx et al. (2013) was built on the astrochronology of the Chaudon-Norante section. Nevertheless, in order to compare both sections with the same resolution, sedimentation rates are also calculated per ammonite Zone (Fig. 6). The sedimentation rates are relatively stable all along the section with a slight decrease in the Propinquans ammonite Zone which is the interval with rarer marlstone beds. The $CaCO_3$ AR is the highest sediment influx even if the clay-rich beds have in some cases a higher siliciclastics AR. As observed in Murtinheira section, siliciclastics and C_{org} ARs have similar trends with a maximum in the Discites ammonite Zone and a slight increase in the upper part of the Humphriesianum ammonite Zone. Excepted few points, the end of the Concavum

ammonite Zone corresponds to a slight decrease in phosphorus accumulation rates whereas the Discites ammonite Zone corresponds to a slight increase. C_{org}/P_{tot} (molar ratio) is always below the Redfield ratio 1:106. Contrarily to the Murtinheira section, alternative results using the Gradstein et al. (2020) age model are presented in supplementary material (Supplementary fig. 2). This solution is not described in this study.

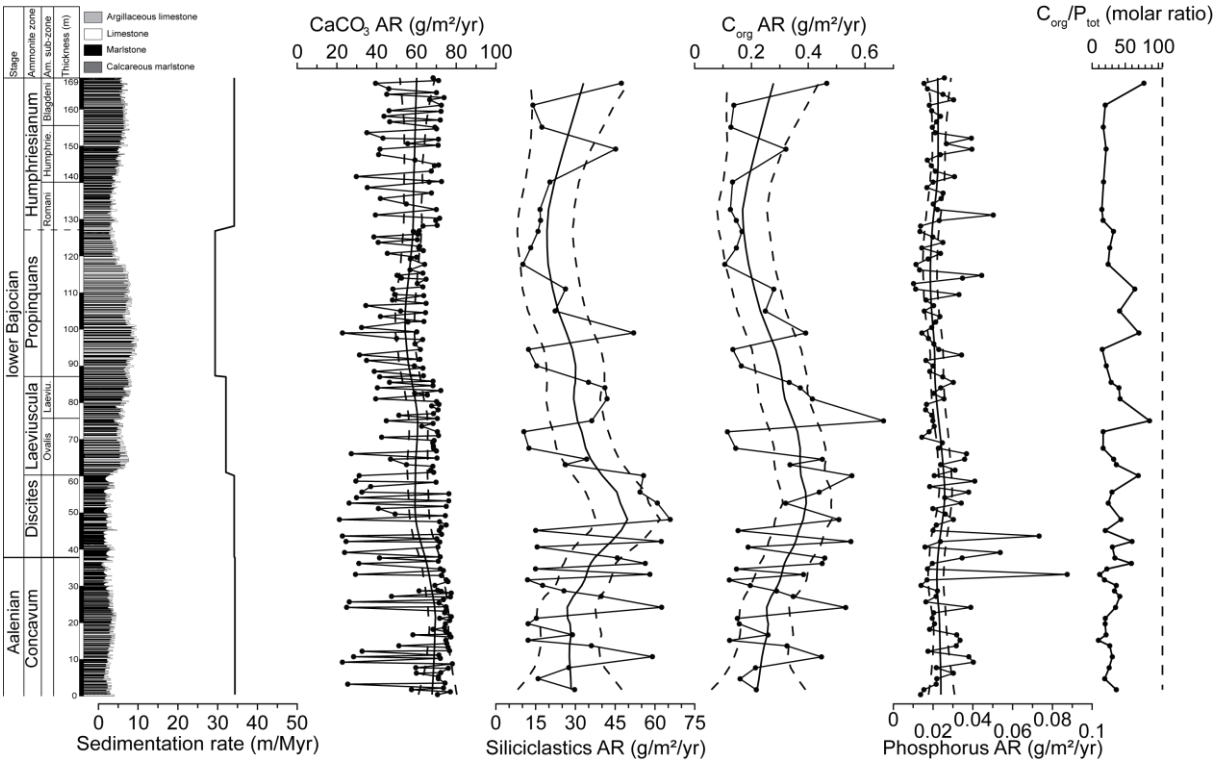

Fig. 6: Stratigraphic changes in sedimentation rate at Chaudon-Norante (based on Suchéras-Marx et al., 2013 age model) and the resulting $CaCO_3$ accumulation rates (AR; g/m²/a), Siliciclastics AR (g/m²/a), C_{org} AR (g/m²/a), and phosphorus AR (g/m²/a), along the C_{org}/P_{tot} molar ratio. The thin lines show the LOESS-smoothed curves (smoothing factor of 0.3) and the 95%CI (dashed lines) calculated using PAST3 (Hammer et al., 2001). The dashed line in C_{org}/P_{tot} data correspond to the Redfield ratio (1:106).

5. Discussion

5.1. The lower Bajocian negative excursion record

The Aalenian-Bajocian boundary is characterized in many sections by a negative CIE (Bartolini et al., 1996; Hesselbo et al., 2003; O'Dogherty et al., 2006; Fantasia et al., 2022). This event is clearly recorded by 0.5‰ negative CIE across the Aalenian-Bajocian in the $\delta^{13}C_{org}$ profile at Chaudon-Norante (Fig. 3) and in Morocco (Fig. 7; Bodin et al., 2017; 2020), but not at Murtinheira (Fig.2). Conversely, the CIE is hardly discernable in bulk carbonate in Chaudon-Norante and in Moroccan sites (Fig. 7), but well-expressed at Murtinheira (Figs. 3 and 7) in the lower part of the Discites ammonite Zone. Discussing the possible causes of this carbon isotope event is thus complicated due to its patchy record in the different localities and carbon substrates. The negative CIE is clearly short-lasting and has a lower amplitude than the ensuing positive CIE (Bartolini et al., 1996; O'Dogherty et al., 2006; Suchéras-Marx et al., 2013). The low magnitude and relatively short duration of this negative CIE may thus partly explain its uneven occurrence among different sites and various types of investigated material. For instance, relatively small changes in proportion of isotopically distinct OM and $CaCO_3$ sources may produce large changes in bulk organic and inorganic records (Swart and Eberli, 2005; Suchéras-Marx et al., 2012; Suan et al., 2015) and may thus have blurred this small negative CIE in some Aalenian-Bajocian bulk records.

5.2. The lower Bajocian positive excursion record

Our new carbon isotope records confirm that the Bajocian positive CIE is present in organic material in Portugal (Fig. 2) and SE France (Fig. 3), and strongly suggest that this geochemical anomaly reflects a perturbation of the global exchangeable carbon reservoir. Indeed, if the positive CIE was only recorded in $\delta^{13}C_{bulk\ carbonate}$, it could have reflected a global shift in the carbonate production i.e., by change in the $CaCO_3$ producers with more positive $\delta^{13}C$ signature (Suchéras-Marx et al., 2012). Conversely, if the $\delta^{13}C_{org}$ positive CIE was recorded only in Morocco (Bodin et al., 2017; 2020), local effect like the carbon residence time in the carbonate platform, or local changes in hydrology, or even change in the source and preservation of the organic matter may have been involved (Suan et al., 2015). Our concomitant record of a positive CIE in both $\delta^{13}C_{bulk\ carbonate}$ and $\delta^{13}C_{org}$ dismiss these hypotheses and confirms the large

368 geographical extent of this carbon cycle perturbation. Our new data suggest that the magnitude
369 of the shift ranges between 1‰ and 1.5‰, in line with previous bulk organic and inorganic
370 records, as well as brachiopod (Ferreira et al., 2019) and belemnite (Jenkyns et al., 2002)
371 records. These latter records have an inherently low resolution and may therefore not fully
372 capture short scale variations in $\delta^{13}C$. Also, changes in proportions of various inorganic and
373 organic particles with distinct $\delta^{13}C$ signatures may greatly distort bulk sediment records (Swart
374 and Eberli, 2005; Suchéras-Marx et al., 2012; Suan et al., 2015). The preliminary qualitative
375 palynological investigations of samples show no major changes in the dominant kerogen type
376 in each section, indicating that the recorded trends are not attributable to changing contribution
377 of distinct type of organic carbon. Nevertheless, our observations indicate that the kerogen is
378 dominated by terrestrial opaque phytoclasts at Murtinheira, whereas phytoclasts and
379 amorphous organic matter (AOM) dominate at Chaudon-Norante. Traditionally, structureless
380 AOM has been considered as derived from bacteria or phytoplankton and strongly altered
381 macrophyte remains (Pacton et al., 2011), this latter source being a volumetrically secondary
382 component in marine sediments (Tyson, 1995). The distal position of the site and non-gelified
383 aspect of the AOM at Chaudon-Norante could therefore indicate a marine source, which was
384 ^{13}C-depleted by 2-4‰ compared to terrestrial phytoclasts during the Jurassic (Suan et al.,
385 2015). Such a ^{13}C-depletion is in good agreement with the 2‰ offset toward lower values of
386 the Chaudon-Norante $\delta^{13}C_{org}$ record relative to that at Murtinheira (Figs. 2 and 3). Accordingly,
387 the $\delta^{13}C_{org}$ record at Chaudon Norante, where ^{13}C-depleted AOM kerogen occurs in higher
388 proportions, could capture a mixed- terrestrial marine signal while the Murtinheira record,
389 where phytoclasts dominate, may essentially captures a terrestrial signal. Such palynological
390 observation are preliminary and qualitative, and further quantification of changing proportions
391 of various inorganic and organic carbon sources will be required to more robustly assess the
392 magnitude of the lower Bajocian positive CIE using bulk records.
393
394 5.3. Similarities with other Mesozoic CIEs

The triggers of the CIEs might be interpreted differently according to their inferred timescales. According to Gradstein et al. (2020), the $\delta^{13}C$ increase interval is more or less lasting the whole Discites and Laeviscula ammonite zones thus corresponding to 580 kyr, and the plateau is lasting 580 kyr. The increasing phase and the plateau have thus the same duration and the whole perturbation lasts a little longer than one million years. The duration of ammonite zones is estimated based on the assumption of an equal duration of subzones and thus it is dependent on the number of subzones in the sub-Boreal zonation scheme (Gradstein et al., 2020). The cyclostratigraphic study of Ikeda et al. (2016) a total duration of ~4 Myr for the Bajocian-Callovian interval, but no other biostratigraphic information is available for the condensed radiolarites section they studied. This poor biostratigraphic age control makes the former results impossible to consider in our framework. According to the cyclostratigraphy established by Suchéras-Marx et al. (2013) at Chaudon-Norante, the positive isotope shift lasted 1.357 Myr and the plateau 2.724 Myr for a total of 4.082 Myr, thus approximately 4 times longer than the duration stated in Gradstein et al. (2020). These differences in the time estimation of the early Bajocian are critical and further data are necessary to definitively get to a consensual solution.

Following the timescale of Suchéras-Marx et al. (2013), the duration of the positive carbon isotope excursion is similar to that of the Weissert event (lasting some 5.84 Myr; Martinez et al., 2015) and much longer than other Mesozoic carbon isotope excursions associated with OAEs, which last around ~1 Myr (e.g., T-OAE, Ait-Itto et al., 2018; OAE1a, Malinverno et al., 2010; OAE2, Boulila et al., 2020). The negative excursion at the Aalenian/Bajocian boundary based on $\delta^{13}C_{org}$ data is estimated to last between 520 kyr and 570 kyr (i.e., 27 cycles of 20 ka or 14 cycles of 37 ka or 41 ka or 5 cyles of 100 ka and 3 cyles of 20 ka). Such a duration seems incompatible with a short-lived event such as asteroid impact or methane clathrates release (e.g., Dickens et al., 1995).

Thus, the carbon isotope perturbations can be described as a ~550 ka negative excursion followed by a positive CIE composed of a phase of increasing values lasting 2.5 times longer than the negative excursion, but shorter than the plateau phase; and a plateau phase ~2 times

longer than the increasing phase. The Aalenian-Bajocian negative CIE observed in several (although not all) records therefore likely reflects a relatively short-lived carbon cycle perturbation, whereas the lower Bajocian positive CIE recorded in bulk carbonate, fossil calcite and organic matter is one of the most pronounced and long-lived carbon cycle perturbations of the Jurassic Period.

Altogether, the long, cumulated duration of the two CIEs is compatible with long-lived geological perturbations, such as tectonically-controlled climatic (e.g., global tectonic, large igneous province) or oceanographic changes (e.g., oceanic connections). The possible mechanisms involved are discussed in the following section.

5.4. Possible environmental drivers of the lower Bajocian positive excursion

5.4.1. Higher fertility and enhanced organic matter burial

Positive CIE in the geological record have been classically attributed to the increased burial of ^{13}C-depleted organic carbon in the oceans, thereby increasing $\delta^{13}C_{DIC}$ values (e.g., Vincent and Berger, 1985; Schlanger et al., 1987). This increased organic carbon burial could reflect higher organic matter production and supply or enhanced preservation in the sediment favored by anoxic conditions and is thus may be partly compatible with some key features of Bajocian sediments despite the fact no black shales are observed in this study. Indeed, the lower Bajocian strata record some of the most important biotic events of the Mesozoic plankton revolution, notably the diversification of the major coccolithophores genus *Watznaueria* (Cobianchi et al., 1992; Giraud et al., 2016), the emergence of planktic foraminifera (BouDagher-Fadel, 2015), an increase in abundance of the dinoflagellate genus *Dissiliodinium* (Wiggan et al., 2018), increase in calcareous nannoplankton accumulation rates (Suchéras-Marx et al., 2015) and derived calcareous nannoplankton $CaCO_3$ (Suchéras-Marx et al., 2012). There is an increase in the geographical distribution of radiolarian deposits (Bartolini et al., 1999) although a major radiolarian turnover is dated earlier in the middle-late Aalenian (Bartolini et al., 1999; Aguado et al., 2008). The early Bajocian is also associated with a major ammonite turnover (O'Dogherty et al., 2006). Moreover, abundant bioclastic deposits of

crinoids and bivalves in carbonate platforms in France and Spain point to the dominance of a filtering community in neritic environments, hence to nutrient-rich surface waters (Dromart et al., 1996; Thiry-Bastien, 2002; Aurell et al., 2003; Brigaud et al., 2009; Molina et al., 2018). Finally, the Chaudon-Norante succession records abundant *Zoophycos* that likely also reflects higher organic matter influx to the sediment (Olivero, 1994). Overall, these paleontological data suggest that strata recording the lower Bajocian positive CIE were deposited during an interval of increased primary productivity. Such an important increase in productivity would have been logically sustained by higher siliciclastic and phosphorus inputs from weathering or increase of widespread upwelling in the western Tethys. The former hypothesis is in line with the major rise of siliciclastic AR and PAR recorded at Murtinheira (Fig. 5), but at odds with the Chaudon-Norante data (Fig. 6) showing a small increase in both siliciclastic AR and C_{org} AR and almost no change in PAR, which could explain the relative low increase in Nannofossil AR. Thus, even if paleontological data suggest a higher primary productivity during the early Bajocian, the fertilization model from continental weathering does not seem fully compatible with the new sedimentological and geochemical data presented here. Conversely, the fertilization could be related to upwelling development in the western Tethys. However, our data cannot unambiguously discriminate between the upwelling model for explaining the ocean fertilization from other mechanisms. According to a previous study on radiolarites, the Western Tethys and Alpine Tethys did not see the development of upwelling-related high productivity, and information about North Atlantic are not available (Baumgartner, 2013).

The lower Bajocian successions investigated in this paper and in previous works (Raucsik, 1999; Bodin et al., 2020) have low to very low TOC contents and C_{org} AR (Figs. 2 and 3, 5 and 6). Furthermore, lower Bajocian strata are unnoticeable in terms of occurrence of petroleum source rock (Kendall et al., 2009). Nevertheless, a stratigraphically thin (~10 cm) black shale level (‘Gaetani level’) at Alpe Turati in Italy has been reported (Erba et al., 2019), which may stratigraphically correspond to part of the increasing phase of the positive CIE. Moreover, “black flysch” have been dated as early Bajocian in Poland, and lower Bajocian black shales have been reported in Alaska (Imlay, 1976; Barski et al., 2012). To our knowledge, however,

the lower Bajocian strata do not yield widespread black shales levels. Importantly, the C_{org}/P_{tot} molar ratios in both studied sites are always lower than the Redfield ratio 1:106 (Figs. 5 and 6), which suggest overall stable, oxic conditions throughout the deposition of the corresponding strata (Suan et al., 2012). This is also coherent with geochemical results from La Losillas section in Spain, which suggest fluctuating but overall oxic conditions during the early Bajocian (Molina et al., 2018). Although investigation of oxygenation conditions and rates of carbon burial in extra-Tethyan sites is warranted, all these data are thus at odds with the hypothesis of increased organic matter preservation under poor oxygenation as the main trigger of the Bajocian CIEs, as proposed for some comparable negative and positive CIEs associated with OAEs.

5.4.2. Carbonate crisis

Alternatively, the positive CIE could be related to a major neritic carbonate crisis, which would have decreased the burial of relatively ^{13}C-enriched material (Bartolini and Cecca, 1999; Bodin et al., 2017). This hypothesis is not supported by our new records showing no major decrease in $CaCO_3$ AR in both sections studied here (Figs. 5 and 6; regardless of the age model used, see SupplFigs. 1-2; Gradstein et al., 2020). However, the carbonate factory was dominated by neritic production by the Middle Jurassic (Suchéras-Marx et al., 2012) thus by carbonate platforms. Hence, the state of productivity in such environments is more critical to evaluate the impact of carbonate burial on the lower Bajocian carbon cycle. In eastern France, the early Bajocian was a period a medium $CaCO_3$ accumulation rates (Dromart et al., 1996). A published compilation of carbonate platforms sedimentation rates does show a peculiar carbonate crisis (Andrieu et al., 2016). The early Bajocian seemed to be an intermediate state between an Aalenian (or upper Aalenian) carbonate production low and a upper Bajocian high (Dromart et al., 1996; Andrieu et al., 2016; Fantasia et al., 2022). This crisis, firstly proposed in Italian platforms (Bartolini and Cecca, 1999), is evidenced by a reduction in $CaCO_3$ accumulation rates in the High Atlas of Morocco (Bodin et al., 2017) and Provence platform of SE France (Léonide et al., 2007). In these regions and in many other carbonate platforms, abundant

crinoids and, to a lesser extent, other filtering organisms are common to dominant carbonate producers during the early Bajocian (e.g. Burgundy-Ardèche, France, Dromart et al., 1996; Lusitanian basin, Portugal, Azerêdo, 1998; Jura, France, Thiry-Bastien, 2002; Basque-Cantabrian and Iberian basins, Spain, Aurell, 2003; Betic basin, Spain, O'Dogherty et al., 2006; Molina et al., 2018; United Arab Emirates, Hönig and John, 2015; northwestern Paris basin, France, Andrieu et al., 2016). This carbonate fossils are associated in many localities with ooids (e.g. Burgundy-Ardèche, France, Dromart et al., 1996; Lusitanian basin, Portugal, Azerêdo, 1998; Jura, France, Thiry-Bastien, 2002; United Arab Emirates, Hönig and John, 2015; northwestern Paris basin, France, Andrieu et al., 2016). Thus, carbonate production in neritic environments was mixed between heterozoan and microbial production (Andrieu et al., 2016) and dominated by grains rather than mud. At Murtinheira and Chaudon-Norante, the carbonate fraction is dominated by mud (Pavia, 1983; Suchéras-Marx et al., 2012) but those pelagic sections are the far reaching end of the carbonate export thus too far to receive grains. Some of the localities recording a marked decrease in carbonate accumulation are also characterized by a relative sea-level rise that could explain local carbonate crisis due to drowning (e.g. Provence, France, Léonide et al., 2007; Morocco, Bodin et al., 2017). The effect of the drowning could have been more effective due to environmental perturbation such as eutrophication. Those conditions may have then favor heterozoan over photozoan platforms. However, heterozoan platforms are less efficient in carbonate production and thus may have been incapable to keep-up. Nevertheless, this carbonate crisis was not global and did not shut down all type of neritic carbonate production and export to the basin. Hence, a carbonate crisis may have contributed to the lower Bajocian positive CIE but was certainly not its main driver.

5.4.3. Data-model comparison

Comparing the $\delta^{13}C_{bulk\ carbonate}$ and $\delta^{13}C_{org}$ in different locality may help to further constrain the possible causes of the positive CIE using the box models proposed by Kump and Arthur (1999). The stratigraphic changes in $\delta^{13}C_{bulk\ carbonate}$ *vs* $\delta^{13}C_{org}$ seem to differ substantially between localities related to local conditions and differences in carbon sources, as mentioned

in section 5.1. However, there are two patterns observed in the three sections shown in Fig. 7, where the $\delta^{13}C_{org}$ profile systematically exhibits a slightly larger positive CIE and an earlier return to pre-excursion values (basal Propinquans ammonite Zone) than that recorded by $\delta^{13}C_{bulk\ carbonate}$. Such a decoupling is incompatible with a simple model of productivity increase driven by a sole increase in phosphate delivery rate to the ocean, which predict a synchronous positive CIE in δ_{org} and δ_{carb} (model fig. 3 in Kump and Arthur, 1999). Our results and published data seem more consistent with a model of coupled increase in rate of riverine phosphate and weathered carbon delivery to the oceans (model fig. 9 in Kump and Arthur, 1999). In the model, the negative CIE results from the enhanced delivery of ^{13}C-depleted carbon from weathering, whereas the increase in organic carbon burial is rather related to the combined effects of higher riverine phosphate delivery initiating the positive CIE and a pCO_2 decrease. Consequently, this version of the model predicts first a ~-0.5‰ negative CIE similar to that observed across the Aalenian-Bajocian boundary followed by a δ_{org} ~1.5‰ positive CIE synchronous with a δ_{carb} ~1‰ positive CIE. Thus, like for the lower Bajocian positive CIE, the CIE amplitude is higher in δ_{org} than in δ_{carb}. Finally, the δ_{org} tends in the model to start decreasing back to pre-CIE values earlier than δ_{carb}, as observed in our sections.

The modelled is driven by a pulse of increased organic matter burial, for which, as mentioned earlier, there is evidence in the early Bajocian. Alternatively, an increase in organic carbon accumulation might have occurred in basins that have not been investigated for their TOC contents or that have since then disappeared. Such an organic matter burial forces a decrease in pCO_2 that would induce a cooling because of counter-greenhouse conditions. This alternative prediction is in line with the ~120 ppm pCO_2 decrease previously calculated for the lower Bajocian between the Aalenian-Bajocian boundary and the Propinquans ammonite Zone (Bodin et al., 2020). This is also in line with the paleotemperature estimates based on $\delta^{18}O$ of brachiopods at Murtinheira, which suggest a 2.5°C cooling (i.e., ~0.5‰ increase in $\delta^{18}O$; Ferreira et al., 2019) of bottom waters in the Propinquans ammonite Zone (Fig. 7). The isotopic data are not perfectly in line with the model in terms of magnitude, which depends on input rates and pCO_2 decrease; besides, according to this model a temperature decrease should

563 rather have occurred in the Discites and Laeviuscula ammonite zones. This discrepancy could
564 be explained by a potential CO_2 increase at the Aalenian-Bajocian boundary, as suggested by
565 stomatal data from the Yorkshire coast (Hesselbo et al., 2003), which would have delayed the
566 temperature decrease, or simply by the relatively low resolution of brachiopod data in this
567 interval. According to bivalve $\delta^{18}O$ data from France, bottom water temperatures increased
568 between Propinquans and Humphriesianum ammonite zones (Brigaud et al., 2009), which
569 could support an increase in pCO_2 following the event of enhanced productivity and burial of
570 organic matter (Kump and Arthur, 1999). This 'cool snap' echoes previous observations based
571 on fossil wood and glendonite occurrences (Philippe and Thevenard, 1996; Price, 1999; Rogov
572 and Zakharov, 2010) suggesting a cooling in the Bajocian *sensu lato*, which would require
573 further stratigraphic refinement. The CO_2 release at the Aalenian-Bajocian boundary related to
574 global plate tectonic and Pacific Ocean plate production (Bartolini and Larson, 2001; Labails
575 et al., 2010) may have induced a rapid warming (Gomez et al., 2009; Korte et al., 2015; Ferreira
576 et al., 2019) at the origin of the increase in the rate of phosphate and weathering carbon release
577 to the oceans from localized riverine input. However, the rate of delivery of limiting elements
578 fertilizing parts of the oceans was slow enough to not have any damaging impact on the oceans
579 like during OAE 2 (i.e., Cenomanian-Turonian boundary). On the contrary, the fertilization
580 promoted diversification and productivity of plankton in the lower Bajocian event (Bartolini et
581 al., 2019; Giraud et al., 2016). The Aalenian to lower Bajocian CIEs are very similar to the
582 Weissert event in term of duration (Martinez et al., 2015), productivity increase (Gréselle et al.,
583 2011; Duchamp-Alphonse et al., 2014; Mattioli et al., 2014; Shmeit et al., 2022) and possible
584 cooling event (Barbarin et al., 2012; Cavaheiro et al., 2021). Thus, a similar cause may be the
585 most probable origin of both these events although it needs to be identified (e.g. volcanic
586 activity proposed by Erba et al. (2004) but excluded by Shmeit et al. (2023)).

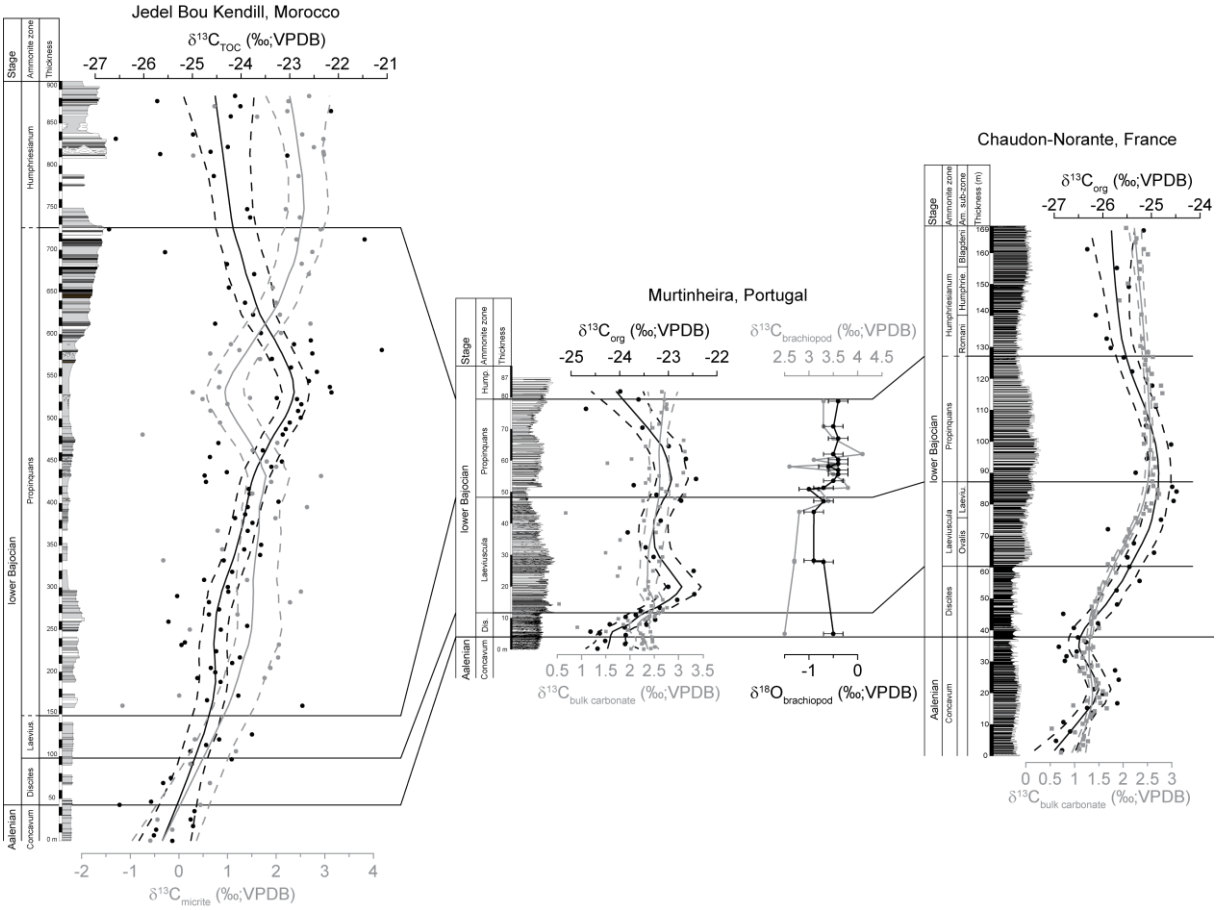

Fig. 7: $\delta^{13}C_{bulk\ carbonate}$ (grey squares; labelled $\delta^{13}C_{micrite}$ in Morocco following Bodin et al., 2017) versus $\delta^{13}C_{org}$ (black circles; labelled $\delta^{13}C_{TOC}$ in Morocco following Bodin et al., 2017) at Jedel Bou Kendill (Morocco), Murtinheira (Portugal) and Chaudon-Norante (France) following a SW-NE transect. At Murtinheira, $\delta^{13}C_{brachiopod}$ (‰, VPDB; grey squares) and $\delta^{18}O_{brachiopod}$ (‰, VPDB; black circles) from Ferreira et al (2019) are plotted. The error bars for $\delta^{18}O_{brachiopod}$ are ±2σ analytical uncertainty.

6. Conclusions

The early Bajocian was a time interval of important biologic, tectonic and climatic perturbations that have been clearly overseen because marine strata deposited during this event lack conspicuous black shale levels and evidence for anoxia. This time interval is also marked by a carbon cycle perturbation in the form of a long-lasting $\delta^{13}C$ positive excursion over the whole lower Bajocian. In France at Chaudon-Norante and in Portugal at Murtinheira, the lower Bajocian $\delta^{13}C$ positive excursion was previously recorded on bulk carbonate and biogenic

602 calcite and is now also recorded on organic matter. This positive excursion reflects a long-lived
603 and marked carbon cycle perturbation likely driven by an increase in organic carbon burial.
604 The studied succession, however, indicate stable organic matter burial fluxes and deposition
605 under stable oxygenation conditions, whereas an increase in erosion and productivity is
606 supported by an increase in siliciclastics AR and PAR only in Murtinheira. The patterns seen
607 in $\delta^{13}C_{bulk\ carbonate}$ and $\delta^{13}C_{org}$ are consistent with those previously described in box model
608 simulating an increase in both riverine flux of phosphorus and inorganic carbon. The Bajocian
609 carbon cycle perturbations fit particularly this solution combining both negative and positive
610 excursions and a cooling period linked to pCO_2 decrease related to an increase in primary
611 productivity. However, this model is clearly too simplistic. There are regional variations in
612 carbonate production with different producers on carbonate platforms (e.g., crinoids,
613 microbialite, scleractinian) between platforms and in biological production with different marine
614 organic producers and amount produced. Those geographical variations complexify the view
615 of the global carbon and environmental perturbation based on too few sites of study.
616 The lower Bajocian event was clearly different from the well-known Cenomanian-Turonian
617 boundary $\delta^{13}C$ positive excursion and bears more similarities with the lower Valanginian $\delta^{13}C$
618 positive excursion characterizing the Weissert event. Further geochemical data and especially
619 more paleotemperature estimates and new sediment data ($CaCO_3$, TOC, P contents) outside
620 the Tethys Ocean are needed to refine the Bajocian carbon cycle perturbation model.
621

622 Acknowledgments

623 BSM thanks Claudine Israel and Théo Mourier for samples decalcification at UJM. BSM thanks
624 Chloé Morales for lodging in Lausanne. We thank Philippe Sorrel for help with palynomorph
625 analyses. The analyses were partly funded by INSU TS SYSTER to EM. This manuscript is a
626 contribution to CEREGE's team Climat.
627

628 Authors' contributions

BSM designed the study based on recommendations from FG, EM, GS and TA. BSM performed the phosphorus analyses in TA's lab at UNIL under the supervision of HMK. AF and JES performed the $\delta^{13}C_{org}$ analyses at UNIL. JCM prepared the organic matter samples at CEREGE and GS performed the observations. BSM and GS interpreted the results. BSM and GS wrote the manuscript with contributions from FG, EM, HMK et AF.

References

Adloff, M., Greene, S.E., Parkinson, I.J., Naafs, B.D.A., Preston, W., Ridgwell, A., Lunt, D.J., Castro Jiménez, J.M., & Monteiro, F.M. (2020). Unravelling the sources of carbon emissions at the onset of Oceanic Anoxic Event (OAE) 1a. *Earth and Planetary Science Letters*, 530, 115947. https://doi.org/10.1016/j.epsl.2019.115947

Aguado, R., O'Dogherty, L., & Sandoval, J. (2008). Fertility changes in surface waters during the Aalenian (mid-Jurassic) of the Western Tethys as revealed by calcareous nannofossils and carbon-cycle perturbations. *Marine Micropaleontology*, *68*, 268-285. https://doi.org/10.1016/j.marmicro.2008.06.001

Aguado, R., O'Dogherty, L., & Sandoval, J. (2017). Calcareous nannofossil assemblage turnover in response to the Early Bajocian (Middle Jurassic) palaeoenvironmental changes in the Subbetic Basin. *Palaeogeography, Palaeoclimatology, Palaeoecology*, *472*, 128-145. http://doi.org/10.1016/j.palaeo.2017.01.044

Ait-Itto, F.-Z., Martinez, M., Price, G.D., & Ait Addi, A. (2018). Synchronization of the astronomical time scales in the Early Toarcian: A link between anoxia, carbon-cycle perturbation, mass extinction and volcanism. *Earth and Planetary Science Letters*, *493*, 1-11. https://doi.org/10.1016/j.epsl.2018.04.007

Al-Mojel, A., Dera, G., Razin, P., & Le Nindre, Y.-M. (2018). Carbon and oxygen isotope stratigraphy of Jurassic platform carbonates from Saudi Arabia: Implications for diagenesis, correlations and global paleoenvironmental changes. *Palaeogeography, Palaeoclimatology, Palaeoecology*, *511*, 388-402. https://doi.org/10.1016/j.palaeo.2018.09.005

Andrieu, S., Brigaud, B., Barbarand, J., Lasseur, E., & Saucède, T. (2016). Disentangling the control of tectonics, eustasy, trophic conditions and climate on shallow-marine carbonate production during the Aalenian–Oxfordian interval : From the western France platform to the western Tethyan domain. *Sedimentary Geology*, *345*, 54-84. https://doi.org/10.1016/j.sedgeo.2016.09.005

Aurell, M., Robles, S., Badenas, B., Rosales, I., Quesada, S., Meléndez, G., & Garcia-Ramos, J.C. (2003). Transgressive-regressive cycles and Jurassic palaeogeography of the northeast Iberia. *Sedimentary Geology*, *162*, 239-271. https://doi.org/10.1016/S0037-0738(03)00154-4

Azerêdo, A. (1998). Geometry and facies dynamics of Middle Jurassic carbonate ramp sandbodies, West-Central Portugal. In V. P. Wright & T. P. Burchette (Eds.), *Carbonate Ramps* (Vol. 149, p. 281-314). Geological Society, London, Special Publications. https://doi.org/10.1144/GSL.SP.1999.149.01.14

Baumgartner, P.O. (2013). Mesozoic radiolarites – accumulation as a function of sea surface fertility on Tethyan margins and in ocean basins. *Sedimentology*, *60*, 292-318. https://doi.org/10.1111/sed.12022

Barbarin, N., Bonin, A., Mattioli, E., Pucéat, E., Cappetta, H., Gréselle, B., Pittet, B., Vennin, E., & Joachimski, M. (2012). Evidence for a complex Valanginian nannoconid decline in the Vocontian basin (South East France). *Marine Micropaleontology*, *84-85*, 37-53. https://doi.org/10.1016/j.marmicro.2011.11.005

Barski, M., Matyja, B.A., Segit, T., & Wierzbowski, A. (2012). Early to Late Bajocian age of the "black flysch" (Szlachtowa Fm.) deposits: implications for the history and geological structure of the Pieniny Klippen Belt, Carpathians. *Geological Quarterly*, *56*, 391-410. https://doi.org/10.7306/gq.1030

Bartolini, A., & Cecca, F. (1999). 20 My hiatus in the Jurassic of Umbria-Marche Apennines (Italy): Carbonate crisis due to eutrophication. *Comptes Rendus Académies des Sciences*, *329*, 587-595. https://doi.org/10.1016/S1251-8050(00)87215-8

684 Bartolini, A., & Larson, R.L. (2001). Pacific microplate and the Pangea supercontinent in the
685 Early to Middle Jurassic. *Geology*, *29*, 735-738.
686 https://doi.org/10.1130/0091-7613(2001)029<0735:PMATPS>2.0.CO;2
687 Bartolini, A., Baumgartner, P.O., & Hunziker, J.C. (1996). Middle and Late Jurassic carbon
688 stable-isotope stratigraphy and radiolarite sedimentation of the Umbria-Marche Basin
689 (Central Italy). *Eclogae Geologicae Helvetiae*, *89*, 811-844. https://doi.org/10.5169/seals-
690 167925
691 Bartolini, A., Baumgartner, P.O., & Guex, J. (1999). Middle and Late Jurassic radiolarian
692 palaeoecology versus carbon-isotope stratigraphy. *Palaeogeography, Palaeoclimatology,*
693 *Palaeoecology*, *145*, 43-60. https://doi.org/10.1016/S0031-0182(98)00097-2
694 Bill, M., O'Dogherty, L., Guex, J., Baumgartner, P.O., & Masson, H. (2001). Radiolarite ages
695 in Alpine-Mediterranean ophiolites: Constraints on the oceanic spreading and the Tethys-
696 Atlantic connection. *Geological Society of America Bulletin*, *113*, 129-143.
697 https://doi.org/10.1130/0016-7606(2001)113<0129:RAIAMO>2.0.CO;2
698 Blättler, C.L., Jenkyns, H.C., Reynard, L.M., & Henderson, G.M. (2011). Significant increases
699 in global weathering during Oceanic Anoxic Events 1a and 2 indicated by calcium isotopes.
700 *Earth and Planetary Science Letters*, *309*, 77-88. https://doi.org/10.1016/j.epsl.2011.06.029
701 Bodin, S., Hönig, M.R., Krencker, F.-N., Danisch, J., & Kabiri, L. (2017). Neritic carbonate crisis
702 during the Early Bajocian: Divergent responses to a global environmental perturbation.
703 *Palaeogeography, Palaeoclimatology, Palaeoecology*, *468*, 184-199.
704 https://doi.org/10.1016/j.palaeo.2016.12.017
705 Bodin, S., Mau, M., Sadki, D., Danisch, J., Nutz, A., Krencker, F.-N., & Kabiri, L. (2020).
706 Transient and secular changes in global carbon cycling during the early Bajocian event:
707 Evidence for Jurassic cool climate episodes. *Global and Planetary Change*, *194*, 103287.
708 https://doi.org/10.1016/j.gloplacha.2020.103287
709 Bomou, B., Adatte, T., Tantawy, A.A., Mort, H., Fleitmann, D., Huang, Y., & Föllmi, K.B. (2013).
710 The expression of the Cenomanian-Turonian oceanic anoxic event in Tibet.

Palaeogeography, Palaeoclimatology, Palaeoecology, *369*, 466-481. http://dx.doi.org/10.1016/j.palaeo.2012.11.011

BouDagher-Fadel, M. K. (2015). The Mesozoic planktonic foraminifera : The Late Triassic–Jurassic. In *Biostratigraphic and Geological Significance of Planktonic Foraminifera* (2e, Revised ed., p. 39-60). UCL Press. https://doi.org/10.2307/j.ctt1g69xwk.6

Boulila, S., Charbonnier, G., Spangenberg, J.E., Gardin, S., Galbrun, B., Briard, J., & Le Callonnec, L. (2020). Unraveling short- and long-term carbon cycle variations during the Oceanic Anoxic Event 2 from the Paris Basin Chalk. *Global and Planetary Change*, *186*, 103126. https://doi.org/10.1016/j.gloplacha.2020.103126

Brigaud, B., Durlet, C., Deconinck, J.-F., Vincent, B., Pucéat, E., Thierry, J., & Trouiller, A. (2009). Facies and climate/environmental changes recorded on a carbonate ramp: A sedimentological and geochemical approach on Middle Jurassic carbonates (Paris Basin, France). *Sedimentary Geology*, *222*, 181-206. https://doi.org/10.1016/j.sedgeo.2009.09.005

Cavalheiro, L., Wagner, T., Steinig, S., Bottini, C., Dummann, W., Esegbue, O., Gambacorta, G., Giraldo-Gómez, V., Farnsworth, A., Flögel, S., Hofmann, P., Lunt, D.J., Rethemeyer, J., Torricelli, S., & Erba, E. (2021). Impact of global cooling on Early Cretaceous high pCO_2 world during the Weissert Event. *Nature Communications*, *12*, 5411. https://doi.org/ 10.1038/s41467-021-25706-0

Cobianchi, M., Erba, E., & Pirini-Radrizzani, C. (1992). Evolutionary trends of calcareous nannofossil genera *Lotharingius* and *Watznaueria* during the Early and Middle Jurassic. *Memorie di Scienze Geologiche, Padova*, *43*, 19-25.

Cohen, K.M., Finney, S.C., Gibbard, P.L., & Fan, J.-X. (2013). The ICS International Chronostratigraphic Chart. *Episodes*, *36*, 199-204. https://doi.org/10.18814/epiiugs/2013/v36i3/002

Corbin, J.-C. (1994). *Evolution géochimique du Jurassique du Sud-Est de la France : influence du niveau marin et de la tectonique*. PhD thesis, Université Paris VI, 198 pp.

738 Dera, G., Brigaud, B., Monna, F., Laffont, R., Puceat, E., Deconinck, J.-F., Pellenard, P.,
739 Joachimski, M.M., & Durlet, C. (2011). Climatic ups and downs in a disturbed Jurassic world.
740 *Geology*, *39*, 215-218. https://doi.org/10.1130/G31579.1
741 Danisch, J., Krencker, F.-N., Mau, M., Mattioli, E., Fauré, P., Alméras, Y., Nutz, A., Kabiri, L.,
742 El Ouali, M., & Bodin, S. (2021). Tracking a drowning unconformity up to the peritidal zone:
743 Proximal expression of the early Bajocian carbonate crisis in Morocco. *Journal of African*
744 *Earth Sciences*, *182*, 104300. https://doi.org/10.1016/j.jafrearsci.2021.104300
745 Dickens, G.R., O'Neil, J.R., Rea, D.K., & Owen, R.M. (1995). Dissociation of oceanic methane
746 hydrate as a cause of the carbon isotope excursion at the end of the Paleogene.
747 *Paleoceanography*, *10*, 965-971. https://doi.org/10.1029/95PA02087
748 Dromart, G., Allemand, P., Garcia, J.-P., & Robin, C. (1996). Variation cyclique de la production
749 carbonatée au Jurassique le long d'un transect Bourgogne-Ardèche, Est-France. *Bulletin*
750 *de la Société Géologique de France*, *167*, 423-433.
751 Duchamp-Alphonse, S., Gardin, S., & Bartolini, A. (2014). Calcareous nannofossil response to
752 the Weissert episode (Early Cretaceous): Implications for palaeoecological and
753 palaeoceanographic reconstructions. *Marine Micropaleontology*, *113*, 65-78.
754 https://doi.org/10.1016/j.marmicro.2014.10.002
755 Erba, E. (1990). Calcareous nannofossil biostratigraphy of some Bajocian sections from the
756 Digne area (SE France). *Memorie Descrittive Della Carta Geologica d'Italia XL*, 237-256.
757 Erba, E. (2004). Calcareous nannofossils and Mesozoic oceanic anoxic events. *Marine*
758 *Micropaleontology*, *52*, 85-106. https://doi.org/10.1016/j.marmicro.2004.04.007
759 Erba, E., & Tremolada, F. (2004). Nannofossil carbonate fluxes during the Early Cretaceous:
760 Phytoplankton response to nutrification episodes, atmospheric CO_2, and anoxia.
761 *Paleoceanography*, *19*, PA1008. https://doi.org/10.1029/2003PA000884
762 Erba, E., Bartolini, A., & Larson, R.L. (2004). Valanginian Weissert oceanic anoxic event.
763 *Geology*, *32*, 149-152. https://doi.org/10.1130/G20008.1

764 Erba, E., Gambacorta, G., & Tiepolo, M. (2019). The Lower Bajocian Gaetani level:
765 Lithostratigraphic marker of a potential oceanic anoxic event. *Rivista Italiana di*
766 *Paleontologia e Stratigrafia*, *125*, 219-230. https://doi.org/10.13130/2039-4942/11390
767 Fantasia, A., Mattioli, E., Spangenberg, J.E., Adatte, T., Bernárdez, E., Ferreira, J., Thibault,
768 N., Krencker, F.-N., & Bodin, S., (2022). The middle-late Aalenian event: A precursor of the
769 Mesozoic Marine Revolution. *Global and Planetary Change, 208*, 103705.
770 https://doi.org/10.1016/j.gloplacha.2021.103705
771 Fernandez-Lopez, S., Henriques, M.H., Mouterde, R., Rocha, R.B., & Sadki, D. (1988). Le
772 Bajocien inférieur du Cap Mondego (Portugal) - Essai de biozonation. In *2nd International*
773 *Symposium on Jurassic Stratigraphy* (p. 301-313). Lisboa.
774 Fernandez-Lopez, S., Pavia, G., Erba, E., Guiomar, M., Henriques, M.H., Lanza, R., Mangold,
775 C., Morton, N., Olivero, D., & Tiraboschi, D. (2009). The Global Boundary Stratotype Section
776 and Point (GSSP) for base of the Bathonian Stage (Middle Jurassic), Ravin du Bès Section,
777 SE France. *Episodes*, *32*, 222-248. https://doi.org/10.1007/s00015-009-1317-1
778 Ferreira, J., Mattioli, E., Sucherás-Marx, B., Giraud, F., Duarte, L.V., Pittet, B., Suan, G.,
779 Hassler, A., & Spangenberg, J.E. (2019). Western Tethys Early and Middle Jurassic
780 calcareous nannofossil biostratigraphy. *Earth-Science Reviews*, *197*, 102908.
781 https://doi.org/10.1016/j.earscirev.2019.102908
782 Friedrich, O., Norris, R.D., & Erbacher, J. (2012). Evolution of middle to Late Cretaceous
783 oceans-A 55 m.y. record of Earth's temperature and carbon cycle. *Geology*, *40*, 107-110.
784 https://doi.org/10.1130/G32701.1
785 Giraud, F., Mattioli, E., López-Otálvaro, G.E., Lécuyer, C., Suchéras-Marx, B., Alméras, Y.,
786 Martineau, F., Arnaud-Godet, F., & de Kænel, E. (2016). Deciphering processes controlling
787 mid-Jurassic coccolith turnover. *Marine Micropaleontology*, *125*, 36-50.
788 https://doi.org/10.1016/j.marmicro.2016.03.001
789 Gomez, J.J., Canales, M.L., Ureta, S., & Goy, A. (2009). Palaeoclimatic and biotic changes
790 during the Aalenian (Middle Jurassic) at the southern Laurasian Seaway (Basque–

Cantabrian Basin, northern Spain). *Palaeogeography, Palaeoclimatology, Palaeoecology*, *275*, 14-27. https://doi.org/10.1016/j.palaeo.2009.01.009

Gradstein, F.M., Ogg, J.G., Schmitz, M.D., & Ogg, G.M. (2020). *Geological time scale 2020* (Vol. 1-2, 1357 pp.). Elsevier, Amsterdam. https://doi.org/10.1016/C2020-1-02369-3

Gréselle, B., Pittet, B., Mattioli, E., Joachimski, M., Barbarin, N., Riquier, L., Reboulet, S., & Pucéat, E. (2011). The Valanginian isotope event: A complex suite of palaeoenvironmental perturbations. *Palaeogeography, Palaeoclimatology, Palaeoecology*, *306*, 41-57. https://doi.org/10.1016/j.palaeo.2011.03.027

Hammer, Ø., Harper, D.A.T., & Ryan, P.D. (2001). PAST: paleontological statistics software package for education and data analysis. *Palaeontologia Electronica*, *4*, 1-9. http://palaeo-electronica.org/2001_1/past/issue1_01.htm

Henriques, M.H., Gardin, S., Gomes, C.R., Soares, A.F., Rocha, R.B., Marques, J.F., Lapa, M.R., & Montenegro, J.D. (1994). The Aalenian-Bajocian boundary at Cabo Mondego (Portugal). In Cresta, S. & G. Pavia (Eds.), *3rd International Meeting on Aalenian and Bajocian Stratigraphy* (p. 63-77). Miscellanea Servizio Geologico Nazionale, Marrakesh.

Hesselbo, S.P., Grocke, D.R., Jenkyns, H.C., Bjerrum, C.J., Farrimond, P., Morgans-Bell, H.S., & Green, O.R. (2000). Massive dissociation of gas hydrate during a Jurassic oceanic anoxic event. *Nature*, *406*, 392-395. https://doi.org/10.1038/35019044

Hesselbo, S.P., Morgans-Bell, H.S., McElwain, J.C., Rees, P.M., Robinson, S.A., & Ross, C.E. (2003). Carbon-cycle perturbation in the middle Jurassic and accompanying changes in the terrestrial paleoenvironment. *The Journal of Geology*, *111*, 259-276. https://doi.org/10.1086/373968

Hönig, M.R., & John, C.M. (2015). Sedimentological and isotopic heterogeneities within a Jurassic carbonate ramp (UAE) and implications for reservoirs in the Middle East. *Marine and Petroleum Geology*, *68*, Part A, 240-257. http://dx.doi.org/10.1016/j.marpetgeo.2015.08.029

Ikeda, M., Bôle, M., & Baumgartner, P.O. (2016). Orbital-scale changes in redox condition and biogenic silica/detrital fluxes of the Middle Jurassic Radiolarite in Tethys (Sogno, Lombardy,

N-Italy): Possible link with glaciation? *Palaeogeography, Palaeoclimatology, Palaeoecology*, *457*, 247-257. https://doi.org/10.1016/j.palaeo.2016.06.009

Imlay, R.W. (1976). Middle Jurassic (Bajocian and Bathonian) ammonites from northern Alaska. *Geological Survey Professional Paper*, *854*, 1-22. https://doi.org/10.3133/pp854

Jarvis, I., Lignum, J.S., Gröcke, D.R., Jenkyns, H.C., & Pearce, M.A. (2011). Black shale deposition, atmospheric CO_2 drawdown, and cooling during the Cenomanian-Turonian Oceanic Anoxic Event. Paleoceanography 26, PA3201. https://doi.org/10.1029/2010PA002081

Jenkyns, H.C., Jones, C.E., Gröcke, D.R., Hesselbo, S.P., & Parkinson, P.N. (2002). Chemostratigraphy of the Jurassic System: applications, limitations and implications for palaeoceanography. *Journal of the Geological Society, London*, *159*, 351-378. https://doi.org/10.1144/0016-764901-130

Kendall, C.G.St.C., Chiarenzelli, J., & Hassan, S.H. (2009). World source rock potential through geological time: A function of basin restriction, nutrient level, sedimentation rate, and sea-level rise. *AAPG Search and Discovery Article #40472*. https://doi.org/10.13140/RG.2.2.16943.69288

Korte, C., Hesselbo, S.P., Ullmann, C.V., Dietl, G., Ruhl, M., Schweigert, G., & Thibault, N. (2015). Jurassic climate mode governed by ocean gateway. *Nature Communications*, *6*, 10015. https://doi.org/10.1038/ncomms10015

Kump, L.R., & Arthur, M.A. (1999). Interpreting carbon-isotope excursions: carbonates and organic matter. *Chemical Geology*, *161*, 181-198. https://doi.org/10.1016/S0009-2541(99)00086-8

Labails, C., Olivet, J.-L., Aslanian, D., & Roest, W.R. (2010). An alternative early opening scenario for the Central Atlantic Ocean. *Earth and Planetary Science Letters*, *297*, 355-368. https://doi.org/10.1016/j.epsl.2010.06.024

Larson, R.L., & Erba, E. (1999). Onset of the Mid-Cretaceous greenhouse in the Barremian-Aptian: Igneous events and the biological, sedimentary, and geochemical responses. *Paleoceanography*, *14*, 663-678. https://doi.org/10.1029/1999PA900040

847 Léonide, P., Floquet, M., & Villier, L. (2007). Interaction of tectonics, eustasy, climate and
848 carbonate production on the sedimentary evolution of an early/middle Jurassic extensional
849 basin (Southern Provence Sub-basin,SE France). *Basin Research*, *19*, 125-152.
850 https://doi.org/10.1111/j.1365-2117.2007.00316.x
851 Malinverno, A., Erba, E., & Herbert, T.D. (2010). Orbital tuning as an inverse problem:
852 Chronology of the early Aptian oceanic anoxic event 1a (Selli Level) in the Cismon
853 APTICORE. *Paleoceanography*, *25*, PA2203. https://doi.org/10.1029/2009PA001769
854 Martinez, M., Deconinck, J.-F., Pellenard, P., Riquier, L., Company, M., Reboulet, S., &
855 Moiroud, M. (2015). Astrochronology of the Valanginian–Hauterivian stages (Early
856 Cretaceous): Chronological relationships between the Paraná–Etendeka large igneous
857 province and the Weissert and the Faraoni events. *Global and Planetary Change*, *131*, 158-
858 173. https://doi.org/10.1016/j.gloplacha.2015.06.001
859 Matsumoto, H., Coccioni, R., Frontalini, F., Shirai, K., Jovane, L., Trindade, R., Savian, J.F.,
860 Kuroda, J. (2022). Mid-Cretaceous marine Os isotope evidence for heterogeneous cause
861 of oceanic anoxic events. *Nature Communications*, 13, 239.
862 https://doi.org/10.1038/s41467-021-27817-0
863 Mattioli, E., Pittet, B., Riquier, L., & Grossi, V. (2014). The mid-Valanginian Weissert Event as
864 recorded by calcareous nannoplankton in the Vocontian Basin. *Palaeogeography,*
865 *Palaeoclimatology, Palaeoecology*, *414*, 472-485.
866 http://dx.doi.org/10.1016/j.palaeo.2014.09.030
867 Molina, J.M., Reolid, M., & Mattioli, E. (2018). Thin-shelled bivalve buildup of the lower
868 Bajocian, South Iberian paleomargin: development of opportunists after oceanic
869 perturbations. *Facies*, *64*, 19. https://doi.org/10.1007/s10347-018-0532-5
870 Monteiro, F.M., Pancost, R.D., Ridgwell, A., & Donnadieu, Y. (2012). Nutrients as the dominant
871 control on the spread of anoxia and euxinia across the Cenomanian-Turonian oceanic
872 anoxic event (OAE2): Model-data comparison. *Paleoceanography*, *27*, PA4209.
873 https://doi.org/10.1029/2012pa002351

874 Mort, H.P., Adatte, T., Föllmi, K.B., Keller, G., Steinmann, P., Matera, V., Berner, Z., & Stüben,
875 D. (2007). Phosphorus and the roles of productivity and nutrient recycling during oceanic
876 anoxic event 2. *Geology*, *35*, 483-486. https://doi.org/10.1130/g23475a.1
877 O'Dogherty, L., Sandoval, J., Bartolini, A., Bruchez, S., Bill, M., & Guex, J. (2006). Carbon-
878 isotope stratigraphy and ammonite faunal turnover for the Middle Jurassic in the Southern
879 Iberian palaeomargin. *Palaeogeography, Palaeoclimatology, Palaeoecology*, *239*, 311-333.
880 https://doi.org/10.1016/j.palaeo.2006.01.018
881 Olivero, D. (1994). La trace fossile *Zoophycos* du Jurassique du Sud-Est de la France.
882 Signification paléoenvironnementale. *Documents des laboratoires de géologie de Lyon*,
883 *129*, 329 pp.
884 Pacton, M., Gorin, G.E., & Vasconcelos, C. (2011). Amorphous organic matter — Experimental
885 data on formation and the role of microbes. *Review of Palaeobotany and Palynology*, *166*,
886 253-267. https://doi.org/10.1016/j.revpalbo.2011.05.011
887 Pavia, G. (1983). Ammoniti e biostratigrafia del Baiociano inferiore di Digne (Francia SE, Dip.
888 Alpes-Haute-Provence). *Monografie Museo Regionale di Scienze Naturali, Torino*, 254 pp.
889 Pavia, G., & Enay, R. (1997). Definition of the Aalenian-Bajocian Stage boundary. *Episodes*,
890 *20*, 16-22. https://doi.org/10.18814/epiiugs/1997/v20i1/004
891 Philippe, M., & Thevenard, F. (1996). Distribution and palaeocology of the Mesozoic wood
892 genus *Xenoxylon*: palaeoclimatological implications for the Jurassic of Western Europe.
893 *Review of Palaeobotany and Palynology*, *91*, 353-370. https://doi.org/10.1016/0034-
894 6667(95)00067-4
895 Pogge von Strandmann, P.A.E., Jenkyns, H.C., & Woodfine, R.G. (2013). Lithium isotope
896 evidence for enhanced weathering during Oceanic Anoxic Event 2. *Nature Geoscience*, *6*,
897 668-672. https://doi.org/10.1038/ngeo1875
898 Price, G.D. (1999). The evidence and implications of polar ice during the Mesozoic. *Earth-*
899 *Science Reviews*, *48*, 183-210. https://doi.org/10.1016/S0012-8252(99)00048-3
900 Raucsik, B. (1999). Clay mineralogy of the Komló Calcareous Marl Formation, Bajocian,
901 Mecsek Mountains, Hungary. *Acta Geologica Hungarica*, *42*, 379-400.

Raucsik, B., Demény, A., Borbély-Kiss, I., & Szabó, G. (2001). Monsoon-like climate during the Bajocian. Clay mineralogical and geochemical study on a limestone/marl alternation (Komló Calcareous Marl Formation, Mecsek Mountains, Southern Hungary). *Hantkeniana*, *3*, 149-176.

Rogov, M.A., & Zakharov, V.A. (2010). Jurassic and Lower Cretaceous glendonites occurrences and their implication for Arctic paleoclimatic reconstructions and stratigraphy. *Earth Science Frontiers*, *Special Issue*, *17*, 345-347.

Ruget-Perrot, C. (1961). Etudes stratigraphiques sur le Dogger et le Malm inférieur du Portugal au Nord du Tage. *Memoria Serviços Geologicos de Portugal*, *7*, 197 pp.

Schlanger, S. O., Arthur, M. A., Jenkyns, H. C., & Scholle, P. A. (1987). The Cenomanian-Turonian oceanic anoxic event, I. Stratigraphy and distribution of organic carbon-rich beds and the marine $\delta^{13}C$ excursion. In J. Brooks & A. J. Fleet (Eds.), *Marine petroleum source rocks* (Vol. 26, p. 371-399). Geological Society Special Publications. https://doi.org/10.1144/GSL.SP.1987.026.01.24

Shmeit, M., Chauvel, C., Giraud, F., Jaillard, E., Reboulet, S., Masrour, M., Spangenberg, J.E., & El-Samrani, A., (2023). Geochemical and radiogenic isotope records of the Weissert Event in south Tethyan sediments. *Journal of the Geological Society*, *180*, jgs2022-023. https://doi.org/10.1144/jgs2022-023

Shmeit, M., Giraud, F., Jaillard, E., Reboulet, S., Masrour, M., Spangenberg, J.E., & El-Samrani, A., (2022). The Valanginian Weissert Event on the south Tethyan margin: A dynamic paleoceanographic evolution based on the study of calcareous nannofossils. *Marine Micropaleontology*, *175*, 102134. https://doi.org/10.1016/j.marmicro.2022.102134

Suan, G., Föllmi, K.B., Adatte, T., Bomou, B., Spangenberg, J.E., & van de Schootbrugge, B. (2012). Major environmental change and bonebed genesis prior to the Triassic-Jurassic mass extinction. *Journal of the Geological Society, London*, *169*, 191-200. https://doi.org/10.1144/0016-76492011-045

Suan, G., Mattioli, E., Pittet, B., Lécuyer, C., Suchéras-Marx, B., Duarte, L.V., Philippe, M., Reggiani, L., & Martineau, F. (2010). Secular environmental precursors to Early Toarcian

(Jurassic) extreme climate changes. *Earth and Planetary Science Letters*, *290*, 448-458. https://doi.org/10.1016/j.epsl.2009.12.047

Suan, G., Pittet, B., Bour, I., Mattioli, E., Duarte, L.V., & Mailliot, S. (2008). Duration of the Early Toarcian carbon isotope excursion deduced from spectral analysis: Consequence for its possible causes. *Earth and Planetary Science Letters*, *267*, 666-679. https://doi.org/10.1016/j.epsl.2007.12.017

Suan, G., van de Schootbrugge, B., Adatte, T., Fiebig, J., & Oschmann, W. (2015). Calibrating the magnitude of the Toarcian carbon cycle perturbation. *Paleoceanography*, *30*, 2014PA002758. https://doi.org/10.1002/2014PA002758

Suchéras-Marx, B., Giraud, F., Fernandez, V., Pittet, B., Lécuyer, C., Olivero, D., & Mattioli, E. (2013). Duration of the Early Bajocian and the associated $\delta^{13}C$ positive excursion based on cyclostratigraphy. *Journal of the Geological Society, London*, *170*, 107-118. https://doi.org/10.1144/jgs2011-133

Suchéras-Marx, B., Giraud, F., Mattioli, E., & Escarguel, G. (2015). Paleoenvironmental and paleobiological origins of coccolithophorid genus *Watznaueria* emergence during the Late Aalenian-Early Bajocian. *Paleobiology*, *41*, 415-435. https://doi.org/10.1017/pab.2015.8

Suchéras-Marx, B., Giraud, F., Mattioli, E., Gally, Y., Barbarin, N., & Beaufort, L. (2014). Middle Jurassic coccolith fluxes: A novel approach by automated quantification. *Marine Micropaleontology*, *111*, 15-25. https://doi.org/10.1016/j.marmicro.2014.06.002

Suchéras-Marx, B., Guihou, A., Giraud, F., Lécuyer, C., Allemand, P., Pittet, B., & Mattioli, E. (2012). Impact of the Middle Jurassic diversification of *Watznaueria* (coccolith-bearing algae) on the carbon cycle and $\delta^{13}C$ of bulk marine carbonates. *Global and Planetary Change*, *86-87*, 92-100. https://doi.org/10.1016/j.gloplacha.2012.02.007

Swart, P.K., & Eberli, G. (2005). The nature of the $\delta^{13}C$ of periplatform sediments: Implications for stratigraphy and the global carbon cycle. *Sedimentary Geology*, *175*, 115-129. https://doi.org/10.1016/j.sedgeo.2004.12.029

Thiry-Bastien, P. (2002). *Stratigraphie séquentielle des calcaires bajociens de l'Est de la France (Jura-Bassin de Paris)*. PhD thesis, Université Claude Bernard Lyon1, Villeurbanne, 407 pp.

Trabucho Alexandre, J., Tuenter, E., Henstra, G.A., van der Zwan, K.J., van de Wal, R.S.W., Dijkstra, H.A., & de Boer, P.L. (2010). The mid-Cretaceous North Atlantic nutrient trap: Black shales and OAEs. *Paleoceanography*, *25*, PA4201. https://doi.org/10.1029/2010pa001925

Tyson, R.V. (1995). Bulk geochemical characterization and classification of organic matter: Stable carbon isotopes ($\delta^{13}C$). In *Sedimentary Organic Matter* (p. 395–416). Springer, Netherlands. https://doi.org/10.1007/978-94-011-0739-6_23

Vincent, E., & Berger, W.H. (1985). Carbon Dioxide and Polar Cooling in the Miocene : The Monterey Hypothesis. In E.T. Sundquist & W.S. Broecker (Eds.), *The Carbon Cycle and Atmospheric CO_2 : Natural Variations Archean to Present* (p. 455-468). Geophysical Monograph Series.

Westermann, S., Stein, M., Matera, V., Fiet, N., Fleitmann, D., Adatte, T., & Föllmi, K.B. (2013). Rapid changes in the redox conditions of the western Tethys Ocean during the early Aptian oceanic anoxic event. *Geochimica et Cosmochimica Acta*, *121*, 467-486. http://doi.org/10.1016/j.gca.2013.07.023

Wiggan, N.J., Riding, J.B., & Franz, M. (2017). Resolving the Middle Jurassic dinoflagellate radiation: The palynology of the Bajocian of Swabia, southwest Germany. *Review of Palaeobotany and Palynology*, *238*, 55-87. https://doi.org/10.1016/j.revpalbo.2016.11.010

Wiggan, N.J., Riding, J.B., Fensome, R.A., & Mattioli, E. (2018). The Bajocian (Middle Jurassic): A key interval in the early Mesozoic phytoplankton radiation. *Earth-Science Reviews*, *180*, 126-146. https://doi.org/10.1016/j.earscirev.2018.03.009

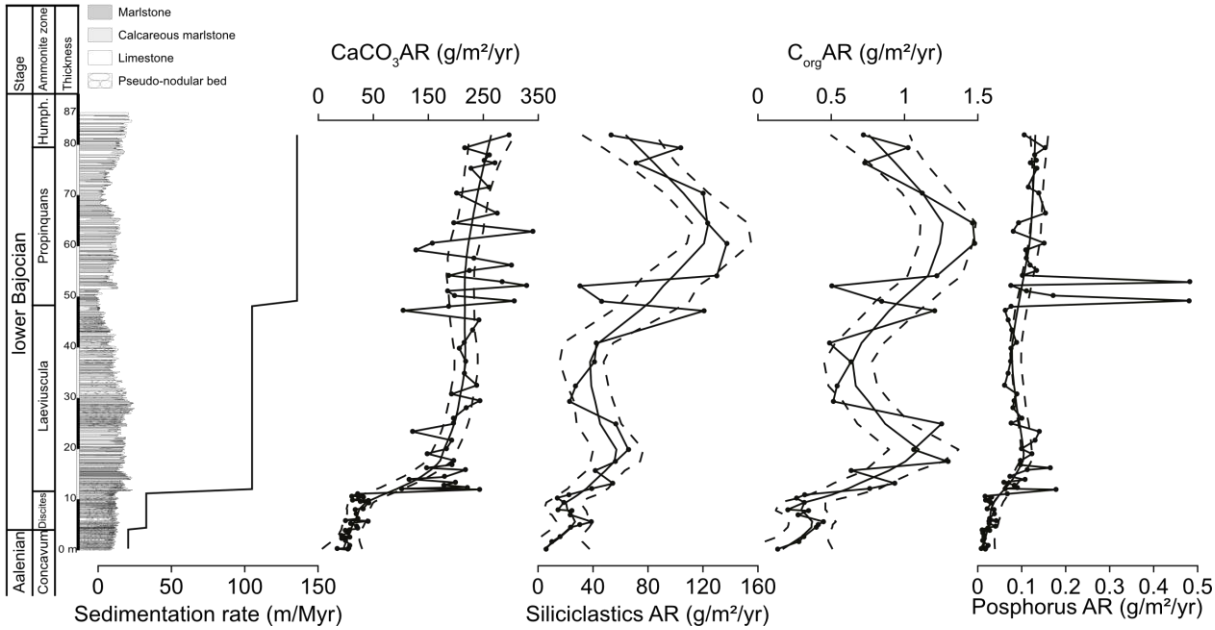

982

983 Supplementary Fig. 1: Stratigraphic changes in sedimentation rate at Murtinheira (based on
984 Gradstein et al. (2020) age model) and the resulting $CaCO_3$ accumulation rates (AR; g/m²/yr),
985 Siliciclastics AR (g/m²/yr), C_{org} AR (g/m²/yr), and phosphorus AR (g/m²/yr).

986

987

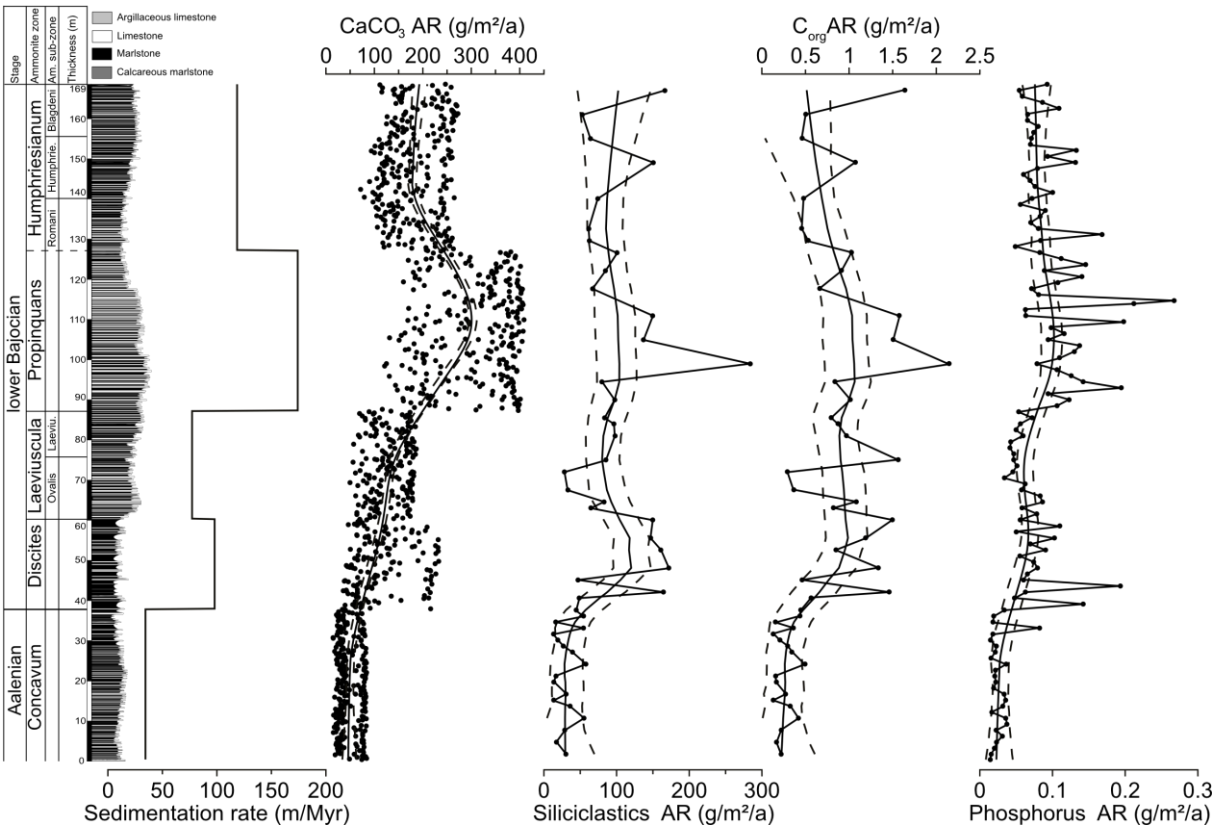

988

Supplementary Fig. 2: Stratigraphic changes in sedimentation rate at Chaudon-Norante (based on Gradstein et al. (2020) age model) and the resulting $CaCO_3$ accumulation rates (AR; $g/m^2/yr$), Siliciclastics AR ($g/m^2/yr$), C_{org} AR ($g/m^2/yr$), and phosphorus AR ($g/m^2/yr$).